HCN Regulates Cellular Processes through Posttranslational Modification of Proteins by *S*-cyanylation[1]

Irene García, Lucía Arenas-Alfonseca, Inmaculada Moreno, Cecilia Gotor, and Luis C. Romero[2,3]

Instituto de Bioquímica Vegetal y Fotosíntesis, Consejo Superior de Investigaciones Científicas and Universidad de Sevilla, Avenida Américo Vespucio, 49, 41092 Sevilla, Spain

ORCID IDs: 0000-0001-7586-5664 (I.G.); 0000-0001-6745-1701 (L.-A.); 0000-0003-4272-7446 (C.G.); 0000-0002-2414-4813 (L.C.R.).

Hydrogen cyanide (HCN) is coproduced with ethylene in plant cells and is primarily enzymatically detoxified by the mitochondrial β-CYANOALANINE SYNTHASE (CAS-C1). Permanent or transient depletion of CAS-C1 activity in Arabidopsis (*Arabidopsis thaliana*) results in physiological alterations in the plant that suggest that HCN acts as a gasotransmitter molecule. Label-free quantitative proteomic analysis of mitochondrially enriched samples isolated from the wild type and *cas-c1* mutant revealed significant changes in protein content, identifying 451 proteins that are absent or less abundant in *cas-c1* and 353 proteins that are only present or more abundant in *cas-c1*. Gene ontology classification of these proteins identified proteomic changes that explain the root hairless phenotype and the altered immune response observed in the *cas-c1* mutant. The mechanism of action of cyanide as a signaling molecule was addressed using two proteomic approaches aimed at identifying the *S*-cyanylation of Cys as a posttranslational modification of proteins. Both the 2-imino-thiazolidine chemical method and the direct untargeted analysis of proteins using liquid chromatography-tandem mass spectrometry identified a set of 163 proteins susceptible to *S*-cyanylation that included SEDOHEPTULOSE 1,7-BISPHOSPHATASE (SBPase), the PEPTIDYL-PROLYL CIS-TRANS ISOMERASE 20-3 (CYP20-3), and ENOLASE2 (ENO2). In vitro analysis of these enzymes showed that *S*-cyanylation of SBPase Cys^{74}, CYP20-3 Cys^{259}, and ENO2 Cys^{346} residues affected their enzymatic activity. Gene Ontology classification and protein-protein interaction cluster analysis showed that *S*-cyanylation is involved in the regulation of primary metabolic pathways, such as glycolysis, and the Calvin and *S*-adenosyl-Met cycles.

Hydrogen cyanide (HCN) is a gaseous acid produced in nature by a wide variety of microorganisms such as fungi, bacteria, and algae (Knowles, 1976), as well as in cyanogenic plant food such as almonds (*Prunus dulcis*), millet sprouts (*Panicum miliaceum*), cassava roots (*Manihot esculenta*), or lima beans (*Phaseolus lunatus*), which are capable of accumulating significant amounts of cyanide, produced by the hydrolysis of cyanogenic glycosides (Hanschen et al., 2014; Baskar et al., 2016; Zidenga et al., 2017). Noncyanogenic plant species also produce cyanide as a byproduct of some metabolic processes, such as during camalexin and ethylene biosynthesis (Peiser et al., 1984; Yip and Yang, 1988; Böttcher et al., 2009).

HCN can be partially dissolved in water and dissociates into H^+ and CN^- particularly in basic solutions. Because the cytosolic pH is close to 7, it is expected that cyanide would mostly present as HCN in this compartment, based on its pK of 9.3. The moderate lipid solubility and small size of the HCN molecule allow it to rapidly cross membranes and enter subcellular compartments. The anion cyanide is highly toxic because it reacts with Schiff base intermediates and keto compounds to produce cyanohydrins and nitrile derivatives and because it chelates divalent and trivalent metal ions in metalloproteins. In mitochondria, it can bind to the heme iron of cytochrome c oxidase, inhibiting the functioning of the electron transport chain and acting as a potent inhibitor of respiration (Isom and Way, 1984). Cyanide is also a potent inhibitor of photosynthesis since it binds copper in plastocyanin, thereby inhibiting plastocyanin-dependent electron transport to PSI (Berg and Krogmann, 1975) and dark CO_2 assimilation (Bishop and Spikes, 1955; Trebst et al., 1960). However, cyanide toxicity in chloroplasts occurs in the dark and is partially reversible by illumination in the presence of an electron acceptor (Bishop and Spikes, 1955; Cohen and McCarty, 1976).

[1]This work was supported in part by the European Regional Development Fund through the Agencia Estatal de Investigación grant BIO2016-76633-P. L. A-A. was supported by the Ministerio de Economia y Competitividad through the program of Formación de Personal Investigador.

[2]Author for contact: lromero@ibvf.csic.es.

[3]Senior author.

The author responsible for distribution of materials integral to the findings presented in this article in accordance with the policy described in the Instructions for Authors (www.plantphysiol.org) is: Luis C. Romero (lromero@ibvf.csic.es).

I.G. and L.A-A. performed the experiments; I.G. and L.C.R. designed the experiments and analyzed the data; C.G. and L.C.R. supervised the experiments; I.M. provided technical assistance; L.C.R wrote the article with the contributions of all authors.

www.plantphysiol.org/cgi/doi/10.1104/pp.18.01083

Free cyanide, produced by metabolic pathways or by the degradation of cyanogenic glycosides, is detoxified by rhodanese or primarily assimilated into amino acids by the action of mitochondrial β-cyano-Ala synthase (CAS-C1), a pyridoxal phosphate-dependent enzyme that uses Cys to detoxify cyanide by converting the cyanide and Cys into hydrogen sulfide (H_2S) and β-cyano-Ala (Ressler et al., 1969; Hatzfeld et al., 2000). The H_2S produced in the mitochondria inhibits cytochrome c oxidase as potently as cyanide and requires detoxification by the mitochondrial *O*-acetyl-Ser(thiol) lyase isoform, which catalyzes the incorporation of sulfide into *O*-acetyl-Ser to produce Cys, thus generating a cyclic pathway in the mitochondria (Álvarez et al., 2012; Nicholls et al., 2013).

Despite its toxicity, cyanide has been proposed to act as a regulator of several biological processes such as seed dormancy and germination (Taylorson and Hendricks, 1973; Bethke et al., 2006; García et al., 2014), resistance to fungal and viral infection (Chivasa and Carr, 1998; Wong et al., 2002; Seo et al., 2011), susceptibility to the fungus *Botrytis cinerea*, and increased tolerance to the bacterium *Pseudomonas syringae* pv. *tomato DC3000*, as well as to the beet curly top virus (Lozano-Durán et al., 2012; García et al., 2013). Arabidopsis (*Arabidopsis thaliana*) null mutants of the mitochondrial CAS-C1 accumulate cyanide to apparently nontoxic levels, as the plants are completely viable, but show a root hairless phenotype suggesting a signaling role in root development (García et al., 2010, 2014; Arenas-Alfonseca et al., 2018). The root hair defect is phenocopied by the addition of cyanide to the growth medium and reversed by the addition of the antidote hydroxocobalamin (García et al., 2010; Thompson and Marrs, 2012). A fused CAS-C1-GFP protein under the control of the CAS-C1 promoter clearly localized in mitochondria but showed a tip-preferred localization during root hair growth (Arenas-Alfonseca et al., 2018). Genetic crosses between the *cas-c1* mutant and the *SUPERCENTIPEDE 1* deficient (*scn1*) or *ROOT HAIR DEFECTIVE 2* (*rhd2*) root hair mutants were performed, and the detailed phenotypic and molecular characterization of the double mutants demonstrated that the *scn1* mutation is epistatic to *cas-c1*, and *cas-c1* is epistatic to the *rhd2* mutation, indicating that CAS-C1 acts in the early steps of the root hair development process. In addition, CAS-C1 function is independent of reactive oxygen species (ROS) production and the direct inhibition of nicotinamide adenine dinucleotide phosphate (NADPH) oxidase by cyanide (Arenas-Alfonseca et al., 2018).

Cyanide functions as a signaling molecule in the response to pathogens as indicated by the transient repression of the *CAS-C1* transcript and accumulation of cyanide when plants were infected with an avirulent *P. syringae* pv. *tomato DC3000 avrRpm1* strain (García et al., 2013). Although transient cyanide accumulation in response to specific pathogens can induce a controlled accumulation of ROS for signaling purposes, a direct effect of cyanide as a signaling molecule cannot be excluded. The cyanide ion can attack cystine peptides or disulfides by nucleophilic displacement on a sulfur atom of the disulfide forming a thiocyanate derivative according to the reaction $\text{R-S-S-R} + CN^- \leftrightarrows \text{R-S}^- + \text{R-S-CN}$ which may be considered a redox reaction (Gawron, 1966). This reaction may occur at intra- and/or interchain disulfide linkages at pH 7.0; however, at alkaline pH, the direction of the reaction would be toward the formation of the thiocyanate derivative (Gawron, 1966; Wagner and Davis, 1966).

The reaction of cyanide with cystine-containing proteins results in the formation of an *S*-cyanylated Cys motif that cycles and is subsequently cleaved to release an amino terminal peptide at one end and a 2-imino-thiazolidine-4-carboxylyl COOH-terminal peptide at the other (Catsimpoolas and Wood, 1966; Fasco et al., 2007). The reaction of cyanide ions with disulfide bridges within polypeptides has been considered to be similar to that of other small molecules, such as nitric oxide (NO) or H_2S, that react with Cys residues to produce Cys modifications (Yamasaki et al., 2016; Aroca et al., 2017b, 2018).

In this study, we thoroughly examined the function of cyanide and the enzyme β-cyano-Ala synthase, which regulates the accumulation/detoxification of cyanide, in the physiology of the cell through a proteomic approach. In addition, we analyzed the molecular mechanism by which cyanide can act as a signaling molecule.

RESULTS

Quantitative Proteomic Analysis of Mitochondrial β-cyano-Ala Synthase CAS-C1 Null Mutant

The absence of β-cyano-Ala synthase in the mitochondria results in a slight increase in total cyanide in whole seedlings by 1.5-fold in the null *cas-c1* mutant and a 3-fold accumulation after treatment with the ethylene/cyanide precursor 1-aminocyclopropane-1-carboxylic acid (ACC; García et al., 2010). To thoroughly investigate the role of CAS-C1 in cellular physiology and decipher the functional mechanism that explains the observed phenotype in the *cas-c1* mutant, we characterized the protein composition and relative abundance of root extracts from wild type and *cas-c1* mutants using proteomics SWATH-MS (sequential window acquisition of all theoretical spectra-mass spectrometry) technology.

Protein samples were isolated from root hydroponic cultures using density-gradient centrifugation aiming to obtain a better enrichment of mitochondrial proteins (Supplemental Table S1). Extracted proteins from three biological replicates of the wild type and three from the *cas-c1* mutant line were digested, and the peptide solutions analyzed by a shotgun data-dependent acquisition (DDA) approach to generate the spectral library. After integrating the six datasets, a total of 11,122 peptides (1% false discovery rate [FDR] and 96% confidence) and 1,734 unique proteins (1% FDR) were identified (Supplemental Dataset S1). To quantify them using SWATH acquisition, the same six biological samples were analyzed twice each (technical replicas) by a data-independent acquisition method using the LC gradient and LC-MS equipment described to generate the spectral library, but instead using the SWATH acquisition method described in the "Materials and Methods" section. Therefore, for quantitation, six datasets from wild type and six from *cas-c1* were generated and used for the analysis. The fragment spectra were extracted for the twelve runs, and 2,035 ion transitions, 2,901 peptides, and 1,132 proteins were quantified. From the 1,132 quantified proteins (Supplemental Dataset S2), 551 had significantly different abundances in wild type and *cas-c1* ($P < 0.05$; Supplemental Table S2). From these proteins, 97 were more abundant in the wild type, exhibiting a fold change >1.5, and 71 were more abundant in *cas-c1* with a fold change <0.66. In addition to the differentially abundant proteins, we detected in the spectral library generated by the DDA approach that 354 proteins were only identified in the wild type samples and were below the detection limit in *cas-c1* (Supplemental Table S3), and 282 were only identified in the *cas-c1* samples (Supplemental Table S4).

The 451 proteins that were absent (354 proteins) or less abundant (97 proteins) in *cas-c1* were analyzed based on their assigned functions and classified into 28 functional groups (Supplemental Table S5) using the MapMan nomenclature (Thimm et al., 2004; Klie and Nikoloski, 2012). The most numerous sets corresponded to the general protein group (bin 29), which included 17.1% of the total identified proteins with 77 elements involved in protein degradation (25 elements, primarily of the ubiquitin-proteasome system), protein synthesis (20 elements), subcellular targeting (11 elements) and posttranslational modification (10 elements). Many of the proteins identified are related to pathogen response and biotic stress (Supplemental Fig. S1A), and Gene Ontology (GO) classification highlighted an important group containing proteins involved in signaling (13.3%) with 60 elements. Interestingly, 26 proteins of the receptor kinase family functioning in pathogen response are present in this group and include six Leu-rich repeat protein kinases, six domain of unknown function26 receptor proteins, and two lectin kinases (Supplemental Fig. S1B; Supplemental Table S5). Previous proteomic analyses in potato (*Solanum tuberosum*) and Arabidopsis have also shown the presence of a significant number of protein kinases in plant mitochondria related to communication and signaling (Salvato et al., 2014; Rao et al., 2017). However, some domain of unknown function26 receptors are cytosolic or plasma membrane proteins and were detected in this proteomic analysis because although the protein preparation was enriched in mitochondria, it also contained other membranes and organelles.

The 353 analyzed proteins that were only present (282 proteins) or more abundant (71 proteins) in *cas-c1* compared to the wild type were classified into 28 functional groups using MapMan (Supplemental Table S6). Once again, the most abundant set classified into the protein group with 59 elements involved in protein synthesis (22 elements), protein degradation (14 elements), subcellular targeting (9 elements), and posttranslational modification (9 elements). An overrepresentation test of the GO terms using PANTHER DB's tool (Mi et al., 2017) to examine the abundant proteins showed a 9.52-fold enrichment of proteins involved in the regulation of carbohydrate metabolism, including four nuclear transcription factors NF-YC1, NF-YC3, NF-YC4, and NF-YC9; 9.33-fold enrichment in cellular amino acid catabolism and 7.35-fold enrichment in ras-related proteins involved in phagocytosis and membrane trafficking (Supplemental Table S7).

Finally, to determine the functional relevance of the *CAS-C1* mutation in the physiology and development of the plant, we used the STRING database v10.5 (Szklarczyk et al., 2015) to analyze the protein-protein interaction network of the 353 proteins with increased abundance in *cas-c1* compared to the wild type to determine functional association of those proteins. Using the highest confidence (interaction score 0.900), a total of 295 protein-protein interactions were observed, and they were significantly enriched (P value < 0.000655) based on the given protein nodes. At least four protein clusters that are biologically connected were clearly distinguished after analysis (Fig. 1). The first cluster contains a subgroup with a complex of 17 ribonucleoproteins (yellow nodes) linked to a second cluster of eight proteins of the spliceosome pathway (red nodes), which is also connected through the E3 ubiquitin ligase MAC3B component of the MOS4-associated complex to a subgroup containing several cyclin-dependent kinases (CDKC1, CDKC2, CDKD1, CDKD3) and ubiquitin-specific protease12 and 13 (UBP12, UBP13). A third important cluster (blue nodes) centered in ELICITOR ACTIVATED GENE3-2 and CYP84A1 (ferulic-acid 5-hydrolase), both involved in lignin biosynthesis, comprises eight peroxidase proteins (PER7, PER16, PER23, PER27, PER32, PER44, PER45, and PER49) and IRX4 (cinnamoyl CoA-reductase, involved in the latter stages of lignin biosynthesis). The fourth cluster (green nodes), centered on RAB GTPas-1A, comprises several subgroups with proteins involved in the endomembrane system, regulators of membrane traffic from the Golgi apparatus toward the endoplasmic reticulum, and includes RAB GTPase-1b, 1c, and 8C and five coatomer subunit proteins. This cluster also contains a subgroup formed by four nuclear transcription factors, NF-YC1, NF-YC3, NF-YC4, and NF-YC9 that regulate gene expression by modulating histone acetylation and methylation.

Identification of *S*-cyanylation by the Chemical 2-Imino-Thiazolidine Method

The cyanide molecule possesses physico-chemical characteristics similar to well-established signaling molecules such as NO, CO, or H_2S (Gotor et al., 2017).

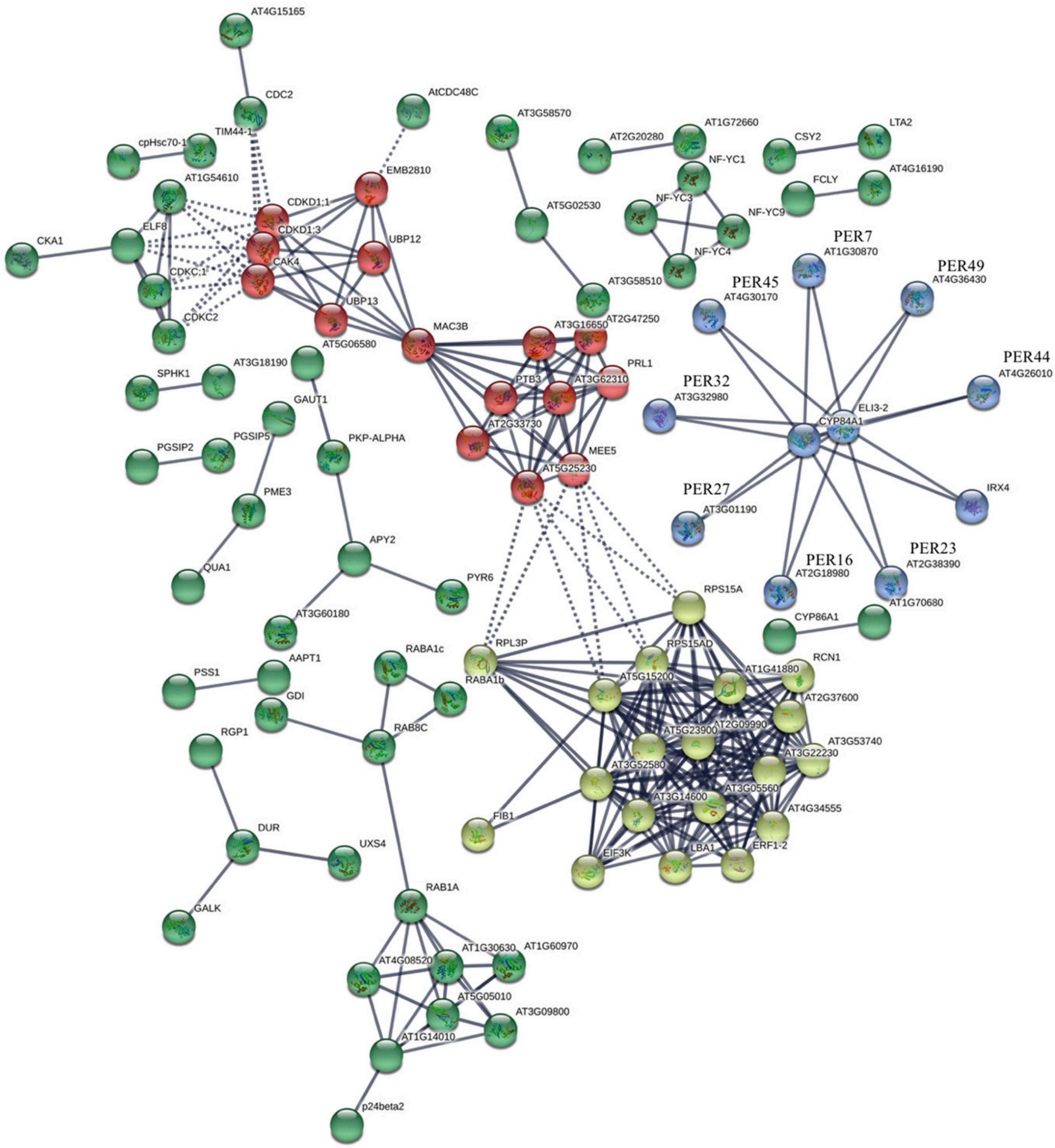

Figure 1. Protein-protein interaction network of the abundant proteins in mitochondrial *cas-c1* samples. Round nodes represent proteins, and lines represent interactions. Dashed lines represent intercluster edges. Node modules indicated in red, yellow, blue, and green were identified by *k*-means clustering.

In addition to its affinity for metalloproteins, cyanide does not react with free thiol groups but can react with cystine-containing proteins at cellular neutral and mild alkaline pH and, by analogy to NO or H_2S, modify protein residues, which subsequently alters protein function. To explore the function of cyanide as a signaling molecule through protein posttranslational modifications (PTMs), we studied the presence of proteins with *S*-cyanylated-Cys residues in cytosolic leaf and root extracts.

It is well described that *S*-cyanylated proteins can be cleaved into two parts, the amino acid backbone from the N terminus to the cyanylated Cys residue and the cycled 2-imino-thiazolidine-4-carboxylyl COOH-terminal peptide (Fig. 2A; Catsimpoolas and Wood, 1966; Fasco et al., 2007), a process that is favored at alkaline conditions. Considering the above chemical properties of *S*-cyanylated cysteines, we studied in vitro the endogenous presence of this modification in leaf protein extracts from Arabidopsis wild-type and *cas-c1* mutant lines. Depletion of CAS-C1 activity results in the accumulation of cyanide in 2-week-old seedlings, and this accumulation can be increased by treatment with ACC, the precursor of ethylene and cyanide, via ACC oxidases (García et al., 2010). Therefore, the presence of endogenous *S*-cyanylated proteins was analyzed in 2-week-old wild-type and *cas-c1* leaves treated with 100 μM ACC for 24 h by comparing the mobility shift or spot volume of the proteins after cleavage with 1 M NH_4OH (Fig. 2B) by the 2-imino-thiazolidine chemical method. The protein samples from 2-week-old leaves were treated with NH_4OH for 1 h or 0.01 M NaOH as a control and separated by two-dimensional (2D) isoelectric focusing sodium dodecyl sulfate-polyacrylamide gel electrophoresis (IEF-SDS-PAGE). Three replicate samples were subjected to 2D IEF-SDS-PAGE, stained with Coomassie Blue, scanned by a densitometer, and the protein spots quantified using image analysis software (Fig. 2B). More than 400 protein dots were resolved in the 2D gel, and 42 proteins in the three replicates from the wild-type leaves showed different electrophoretic mobility or spot volume after alkaline digestion with NH_4OH compared to the control samples at mild alkaline treatment, and the number increased to 72 in the *cas-c1* leaf samples, resulting in 88 different proteins (Supplemental Table S8). Twenty-six proteins were present in both genetic backgrounds, suggesting that *S*-cyanylation may occur independently of the absence or presence of β-cyano-Ala synthase activity after the induction of ethylene synthesis. Interestingly, one of these proteins was 1-AMINOCYCLOPROPANE-1-CARBOXYLATE OXIDASE2, which is responsible for the cobiosynthesis of ethylene and cyanide from ACC. Two of the proteins with different electrophoretic mobility were the chloroplastic sedoheptulose-1,7-bisphosphatase (SBPase) and the peptidyl-prolyl cis-trans isomerase (CYP20-3; Fig. 2B).

GO term enrichment analysis for biological processes using the PANTHER DB's tool (Mi et al., 2017) showed an overrepresentation among *S*-cyanylated proteins of those involved in glycolysis, with a 65-fold enrichment, and in the Calvin cycle. The GO analysis of *S*-cyanylated proteins by cellular components in the *cas-c1* lines showed an enrichment in proteins of the phosphopyruvate hydratase complex, including ENOLASE1 and 2 (ENO1 and ENO2) with >100-fold enrichment (Supplemental Table S9), which are known to be associated with other glycolytic enzymes on the surface of Arabidopsis mitochondria (Giegé et al., 2003).

Identification of *S*-cyanylation by Mass Spectrometry

To further evaluate the presence of this modification in the Arabidopsis proteome, we also analyzed the presence of *S*-cyanylated cysteines in root tissues from wild-type plants using mass spectrometry to

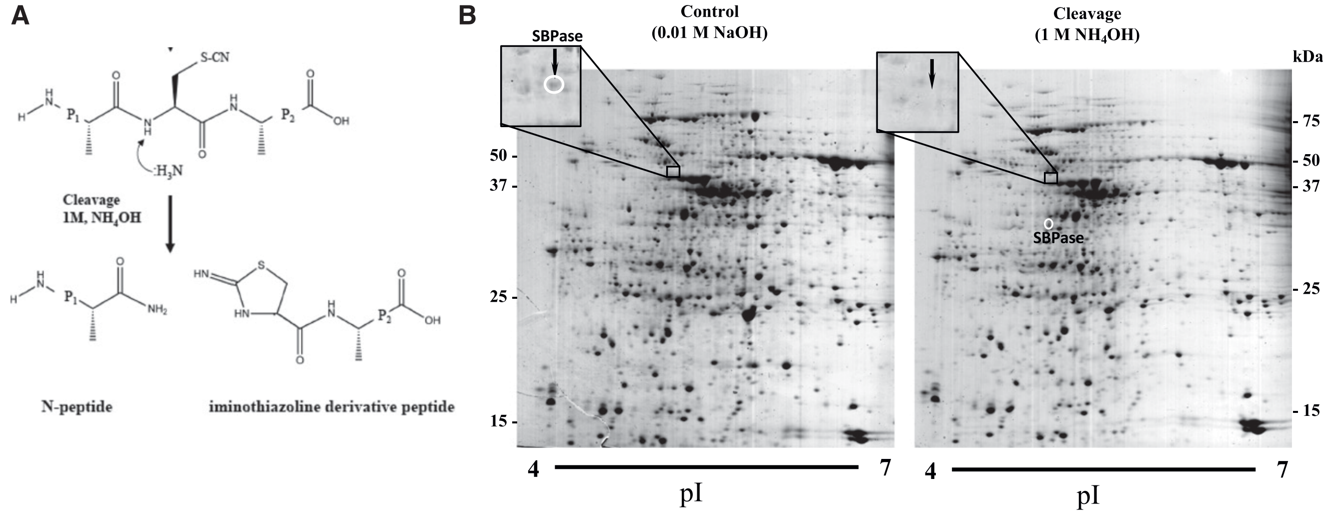

Figure 2. Cyanylation and in vitro analysis in leaf samples. A, Chemical cleavage of the peptide chains on the N-terminal side of cyanylated Cys residues. *S*-cyanylated peptide at alkaline pH results in the cleavage of the protein into two peptides: the N-terminal backbone at the Cys-CN residue and a cycled iminothiazoline derivative peptide. B, Representative 2D IEF-SDS-PAGE protein profile of protein extracts of 2-week-old Arabidopsis *cas-c1* mutant leaves treated with 100 μM ACC for 24 h. Proteins were treated with 0.01 M NaOH (control samples) or 1 M NH_4OH and were separated in the first dimension in gel strips (7 cm) with a linear pH gradient 4 to 7 and in 12% acrylamide vertical gels in the second dimension and stained with Coomassie Blue G-250. White circles show the mobility shift of a representative protein (SBPase).

complement the chemical 2-imino-thiazolidine method. For this purpose, we compared root tissues untreated or treated with ACC as a generator of cyanide and utilized high-resolution MS to determine the presence of peptides containing Cys residues with cyanide modification, which would result in a 25.0095 D mass increase in the fragmentation spectrum. Although this modification has been poorly studied, there are some reports that have detected *S*-cyano-Cys modifications using mass spectrometry (Bishop and Spikes, 1955; Fricker, 2015). For protein identification, we used three biological replicate samples of total protein extracts from root tissues untreated or 100 μM ACC-treated for 24 h and identified a total of 2,442 proteins present in the three replicates of treated roots and 2,325 in the three replicates of the untreated samples (Supplemental Dataset S3). From these, 30 proteins in the untreated roots and 50 proteins in the treated roots, representing 64 different proteins, were found to contain an *S*-cyanylation-Cys modification. A total of 67 peptides were identified from the 64 different proteins, which constitute 1.4% of the proteins identified in roots (Table 1). Moreover, in the SWATH proteomic analysis described earlier, we identified 11 additional peptides that were modified by *S*-cyanylation, which were added to the list of proteins identified using LC-MS/MS (Supplemental Table S10).

All the proteomic approaches described in this study have allowed us to identify a total of 163 different proteins susceptible to *S*-cyanylation: 88 unique proteins using the 2-imino-thiazolidine chemical method and 75 proteins using the LC-MS/MS method (Supplemental Table S10). The *S*-cyanylated proteins identified were analyzed based on their assigned functions and classified into 28 functional groups using the MapMan nomenclature. The most abundant set corresponded to the general protein group, which included 13% of the total identified proteins with 22 elements, and the photosynthesis bin with 19 elements, which included the small and the large subunit of Rubisco and several other enzymes of the Calvin cycle and glycolysis including ENO1 and ENO2.

To examine the function of *S*-cyanylation in metabolism and regulatory processes in more detail, the 163 *S*-cyanylated proteins were analyzed using the STRING database v10.5. Using the highest confidence (interaction score 0.900), a total of 193 protein-protein interactions were observed, and they were significantly enriched (P value $< 1.0\ e^{-16}$) based on the given protein nodes, suggesting that they are biologically connected. *k*-means clustering analysis of the protein-protein interaction network identified four clusters of proteins with important biological functions (Fig. 3). The cluster containing the most proteins (red nodes) includes proteins involved in several metabolic processes such as protein folding, including CHAPERONIN-60ALPHA, CHAPERONIN-60BETA2, chloroplast and mitochondrial heat shock proteins HSP70-1 and HSP70-2, ROTAMASE FKBP-1, and other HSPs; the TCA cycle, including ACONITASE1 and 2 (AT4G26970); isocitrate dehydrogenases (ICDH and cICDH), and response to stress including the beta-glucosidases BGLU21, BGLU22, BGLU23/PYK10. Members of this group (RBCL and RBCS) are connected to a second cluster (yellow nodes), which includes proteins involved in carbon fixation and glycolysis/gluconeogenesis, such as ENO1 and ENO2/LOS2, GLYCERALDEHYDE-3-PHOSHPHATE DEHYDROGENASE A, and several phosphoglycerate kinases and aldolases (Fig. 3; Supplemental Fig. S2). A third cluster (blue nodes) comprises enzymes of the *S*-adenosyl Met cycle centered in MET OVER-ACCUMULATOR3, essential in DNA and histone methylation, and includes DNA METHYLTRANSFERASE2 (DMT2), MET SYNTHASE1 and 2 (ATMS1, ATMS2) and *S*-ADENOSYL-L-HOMOCYSTEIN HYDROLASE1 (SAHH1). The last cluster (green nodes) contains several ribosomal proteins involved in protein synthesis.

Identification of *S*-cyanylated Cys Residues of Representative Proteins

To demonstrate that Cys residues are indeed modified by *S*-cyanylation and to identify the modified residues of representative proteins identified by the chemical 2-imino-thiazolidine method, we conducted LC-MS/MS analyses of SBPase and CYP20-3. Recombinant proteins were purified from bacterial extracts and trypsin-digested, and the digested peptides were analyzed using LC-MS/MS to identify a 25.0095 D mass increase in the fragmentation spectrum. As illustrated in Figure 4 (Supplemental Table S11), the SBPase enzyme was identified with a sequence coverage of 67% and among the peptides identified, the peptide SNGASTVTKCEIGQSLEEFLAQATPDK, containing Cys^{74}, showed *S*-cyanyl modification. The Cys^{116} and Cys^{121} residues that form a disulfide bridge and can be redox regulated by thioredoxin f were not detected as *S*-cyanylated. In the same manner, as SBPase, the CYP20-3 protein was analyzed by LC-MS/MS. The protein was identified with a sequence coverage of 61% and Cys^{206} within the peptide HTGPGILSMANAGPNTNGSQFFICTVK was identified as *S*-cyanylated (Fig. 5; Supplemental Table S12). The activity of CYP20-3 is controlled by thioredoxin-mediated redox regulation of the two disulfide bridges between Cys^{131}-Cys^{248} and Cys^{206}-Cys^{253} and the enzyme is fully enzymatically inactive in the oxidized state (Motohashi et al., 2003). The redox state of CYP20-3 was determined by analysis of the redox-dependent electrophoretic mobility of the protein under oxidizing and reducing conditions. Proteins with reduced Cys residues can be alkylated and therefore run more slowly during electrophoresis than oxidized proteins that cannot be alkylated. Treatment with H_2O_2 oxidized the Cys residues of CYP20-3 inducing formation of disulfide bridges, which changed its mobility such that it migrated more quickly than the reduced and iodoacetamide-alkylated protein (Fig. 6A). When the oxidized protein was subsequently treated with cyanide, its mobility was reduced due to the

Table 1. *S-cyanylated Proteins and Peptides Identified in Total Protein Extracts from Root Tissues by Untargeted LC-MS/MS Analysis*

AGI locus	Description	*S*-cyanylated Peptide
At1g07890	Ascorbate peroxidase APX1	GLIAEKNCAPIMVR
At1g12820	Auxin signaling F-box 3 protein AFB3	SLWMSSCEVTLGGCK (2 Cyano)
At1g15890	Disease resistance protein (CC-NBS-LRR class) family	QKETLCVK
At1g35720	Member of the annexin gene family ANN1	STIQCLTRPELYFVDVLR
At1g52150	Homeobox-Leu zipper protein AtHB-15	ECPILSNIEPK
At1g53310	Phosphoenolpyruvate carboxylase PPC1	SLCSCGDRPIADGSLLDFLR
At1g54340	NADP-specific isocitrate dehydrogenase ICDH	LVPGWTKPICIGR
At1g60810	ATP-citrate lyase ACLA-2	LGCSISFSECGGIDIEENWDKVK
At1g64190	6-phosphogluconate dehydrogenase PGD1	ICSYAQGMNLLR
At1g65930	Cytosolic isocitrate dehydrogenase [NADP]	CATITPDEGRVTEFGLK
		CATITPDEGR
		LVPGWTKPICIGR
At2g01520	MLP328	IWNYTCDGKPEVFK
At2g01530	MLP329	IWNYTCDGKPEVFK
At2g17360	40S ribosomal protein S4-1	SRECLPLVLIIR
At2g17420	NADPH-dependent thioredoxin reductase NTR2	VCIVGSGPAAHTAAIYASR
At2g20420	ATP citrate lyase (ACL) family protein	CDVIASGIVNAAK
At2g21660	Small Gly-rich RNA binding protein CCR2	CFVGGLAWATDDR
At2g31610	40S ribosomal protein S3-1	GLCAIAQAESLR
At2g34220	Maternal effect embryo arrest 20, MEE20	CFLSVVR
At2g36530	Enolase ENO2/LOS2	SCNALLLK
At2g45290	Transketolase TKL2	NLSQQCLNALAK
At2g48060	piezo-type mechanosensitive ion channel component	VECRMNQLLR
At3g02360	6-phosphogluconate dehydrogenase PGD2	ICSYAQGMNLIR
At3g03670	Peroxidase superfamily protein	MHFHDCFVQGCDASLLIDPTTSQLSEK
At3g03780	Met synthase MS2	CVKPPVIYGDVSRPK
At3g05590	60S ribosomal protein RPL18	AGGECLTFDQLALR
At3g11670	Digalactosyldiacylglycerol synthase 1	AYCDKVLR
At3g19390	Granulin repeat Cys protease family protein	CGVAMMASYPTK
At3g22860	Eukaryotic translation initiation factor 3 subunit C	AMLCDIYQHALMDNFVTAR
At3g23600	Alpha/beta-hydrolases superfamily protein	SGPQCCENPPTLNPVSGSGHVEK
At3g23810	S-adenosyl-l-homo-Cys hydrolase ATSAHH2	VAVICGYGDVGK
At3g27430	20S proteasome beta subunit PBB1	TEGPIVADKNCEKIHYMAPNIYCCGA
		GTAADTEAVTDMVSSQLR
At3g32980	Peroxidase family protein	TVSCADILTIAAQQAVNLAGGPSWR
At3g48340	KDEL-tailed Cys endopeptidase CEP2	CGIAMEASYPIK
At3g48990	4-coumarate-CoA ligase-like 10	SCSASLAPVILSR
At3g53870	40S ribosomal protein S3-2	GLCAIAQAESLR
At3g57610	Adenylosuccinate synthetase (AdSS)	CQGGANAGHTIYNSEGKK
At3g60750	Transketolase ATTKL1	NLSQQCLNALAK
		SGHPGLPMGCAPMAHILYDEVMR
At4g13930	Ser hydroxymethyltransferase SHM4	LLICGGSAYPR
At4g13940	S-adenosyl-L-homo-Cys hydrolase HOG1	VAVICGYGDVGK
At4g14140	DNA methyltransferase DMT2	CGIAMEASYPIK
At4g22970	Separase-like protein ESP/RSW4	CAVSLVR
At4g26970	Aconitase ACO2	SFVCTLRFDTEVELAYYDHGGILPYVIR
At4g34870	Rotamase cyclophilin CYP18-4/ROC5	VIPGFMCQGGDFTAK
At4g35830	Aconitase ACO1	SFTCTLRFDTEVELAYFDHGGILQYVIR
At5g07660	Structural maintenance of chromosomes protein 6A	ERVPTCQNKIDR
At5g11670	NADP-dependent malic enzyme NADP-ME2	TYLPGQANNCYIFPGLGLGLIMSGAIR
At5g11920	Protein with fructan exohydrolase activity	CLIDHSIIESYGVGGK
At5g12080	Mechanosensitive ion channel ATMSL10	VLKCITR
At5g14590	Isocitrate dehydrogenase	CATITPDEGR
At5g16210	HEAT repeat-containing protein	IIMDACVSLSR
At5g17920	Met synthase ATMS1	CVKPPVIYGDVSRPK
At5g20160	Ribosomal protein L7Ae/L30e/S12e/Gadd45	ACGVTRPVIACSVTSNEASQLK
At5g27850	60S ribosomal protein L18-3	AGGECLTFDQLALR
At5g35530	40S ribosomal protein S3-3	GLCAIAQAESLR
At5g40580	20S proteasome beta subunit PBB2A	TEGPIVADKNCEKIHYMAPNIY
		CCGAGTAADTEAVTDMVSSQLR
At5g41670	6-phosphogluconate dehydrogenasePGD3	ICSYAQGMNLLR

(*Table continues on following page.*)

Table 1. (*Continued from previous page.*)

AGI locus	Description	*S*-cyanylated Peptide
At5g43060	Cys protease family protein RD21B	CGIAMEASYPIKK
At5g45500	RNI-like superfamily protein	CKVTVLR
At5g46850	Phosphatidylinositol-glycan biosynthesis	RCLVLSIGR
At5g52640	Heat shock protein AtHsp90-1	VVVSDRIVDSPCCLVTGEYGWTANMER (2 Cyano)
At5g56000	Heat shock protein AtHsp90-4/Hsp81-4	VIVSDRVVDSPCCLVTGEYGWTANMER (2 Cyano)
At5g56010	Heat shock protein AtHsp90-3/Hsp81-3	VIVSDRVVDSPCCLVTGEYGWTANMER (2 cyano)
At5g56030	Heat shock protein AtHsp90-2/Hsp81-3/ERD8	VIVSDRVVDSPCCLVTGEYGWTANMER (2 cyano)
At5g58420	40S ribosomal protein RPS4A	SRECLPLVLIIR

rupture of the disulfide bridge by *S*-cyanylation. However, rupture of the disulfide bridges by cyanide treatment did not reactivate the enzymatic activity, which could only be partially recovered after reduction with dithiothreitol (DTT; Fig. 6B).

The effect of *S*-cyanylation on ENO2, identified in the two proteomic approaches, was also analyzed. Enolase is a multifunctional enzyme that has catalytic activity in glycolysis, converting 2-phosphoglycerate into phosphoenolpyruvate, and also acts as a regulator of gene transcription (Lee et al., 2002). Arabidopsis ENO2 contains five Cys residues in its sequence, but we found that only Cys^{346} within the peptide SCNALLLK was modified by *S*-cyanylation (Fig. 7; Supplemental Table S13). We measured the effect of oxidation using H_2O_2 treatment and observed a significant increase in enzymatic activity due to Cys oxidation and the resulting formation of disulfide bridges (Fig. 8). This result is consistent with data previously observed for some other plant enolases from Arabidopsis, tomato (*Solanum lycopersicum*), and the ice plant *Mesembryanthemum crystallinum*, which may form a disulfide bridge between Cys^{313} and Cys^{338} (according to the maize [*Zea mays*] sequence) at the C-terminal active site of the enzyme. Its activity can be slightly inhibited by DTT and can be activated approximately 2-fold by the oxidant diamine (Anderson et al., 1998). Further treatment with cyanide after the H_2O_2 oxidation increased the enzymatic activity of the Arabidopsis ENO2 by >50% (Fig. 8). Enolase has been identified to be a target of thioredoxin in several proteomic studies, but in vivo studies and the regulatory Cys residues have not been reported.

DISCUSSION

Changes in the *cas-c1* Proteome Explains the Root Hair Defect and Altered Response to Pathogens

HCN is produced in plants by several metabolic processes, but in noncyanogenic plants, ethylene biosynthesis is thought to be the primary source (Yip and Yang, 1988). Therefore, during many developmental or environmental stress processes where ethylene is produced, the amount of cosynthesized HCN can be substantial. HCN can be removed or detoxified either by enzymatic activities (rhodanese and β-cyano-Ala synthase) or, due its own chemical reactivity, reaction with organic molecules susceptible to nucleophilic attack like disulfide bridges, such as cystine, oxidized glutathione, and organic persulfides, producing the corresponding thiocyanate, and reaction with aldehydes and ketones to produce cyanohydrins (Gawron, 1966; Park et al., 2015). Thus, plants have evolved mechanisms to control cyanide levels and avoid its toxic effects. Although the high reactivity of HCN makes it very toxic, it is interesting to note that transcript levels of *CAS-C1* are transiently repressed, with the corresponding accumulation of cyanide, after infection with an avirulent *Pst* DC3000 *avrRpm1* strain, indicating that there are defined programs in the cell to allow the accumulation of cyanide probably for signaling purposes (García et al., 2013, 2014; Romero et al., 2014). In fact, cyanide has chemical characteristics very similar to other gasotransmitters such as NO, CO, and H_2S and meets all the criteria to be classified as one (Tinajero-Trejo et al., 2013; Wang, 2014).

Together with the quantified changes in root hair growth and pathogen response induced by the *CAS-C1* mutation, molecular phenotyping by proteomic analysis of *cas-c1* can identify pathways that contribute to the observed phenotypic changes (Fig. 1; García et al., 2010, 2013; Arenas-Alfonseca et al., 2018). The decrease in the ability to enzymatically detoxify cyanide in the mitochondria results in the accumulation of proteins involved in the initial elongation phase of root hair growth, such as GTPases and cell wall modification enzymes (Grierson et al., 2014). One of these groups includes RAB GTPase-1A, other RAB GTPases, and several coatomer subunit proteins, which function in the endomembrane system to regulate membrane traffic from the Golgi apparatus toward the endoplasmic reticulum. Since the polarized expansion of root hairs depends on the formation and delivery of cell wall components to the growing tips, changes in the RAB GTPase composition and activity may alter the formation and delivery of secretory vesicles from the trans-Golgi network. In addition to the membrane trafficking protein clusters, the *CAS-C1* mutation regulates and induces the accumulation of groups of proteins involved in lignin biosynthesis for cell wall formation, which suggests an increased accumulation of lignin that may inhibit or hinder the cell wall relaxation for tip growth. Previous transcriptional data from root tissues (García et al., 2010) revealed the repression of several

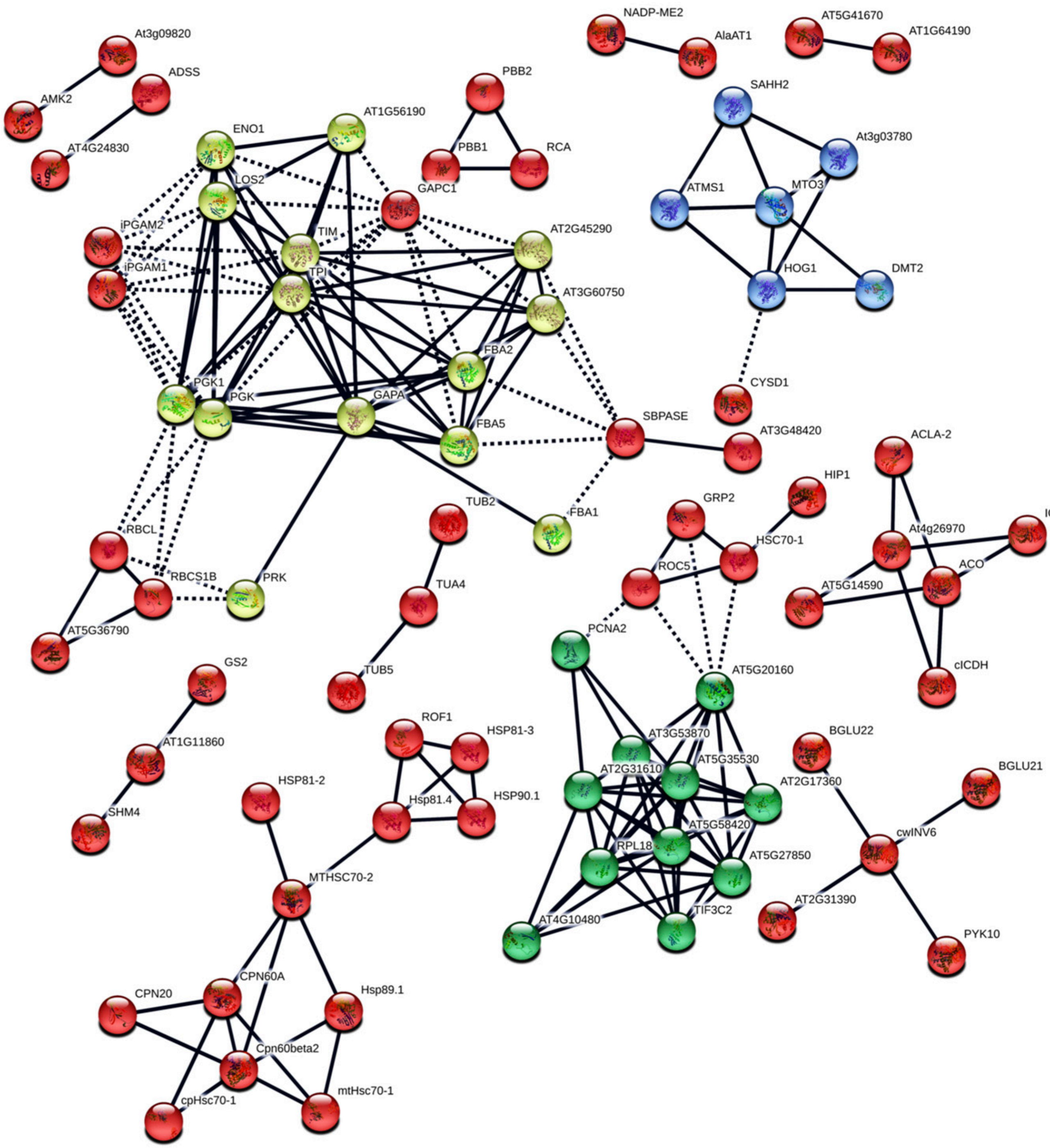

Figure 3. Protein-protein interaction network of identified *S*-cyanylated proteins in leaf and root tissues. Round nodes represent proteins, and lines represent interactions. Dashed lines represent intercluster edges. Node modules indicated in red, yellow, blue, and green were identified by *k*-means clustering.

well-known genes related to root hair formation, such as *MRH5/SHV3*, *MRH6*, and *XTR9*, encoding arabinogalactan proteins, xyloglucan:xyloglucosyl transferases, endotransglycosylase, pectinesterases, and pectate lyase proteins that have been correlated with the organization of cortical microtubules that influence root epidermal expansion and morphogenesis (Nguema-Ona et al., 2007). Since the site of bulge formation requires that the trichoblast locally loosens its cell wall, this process must be interfered with in *cas-c1.* Transcriptomic and proteomic data are thus consistent with the interpretation that cyanide regulates root

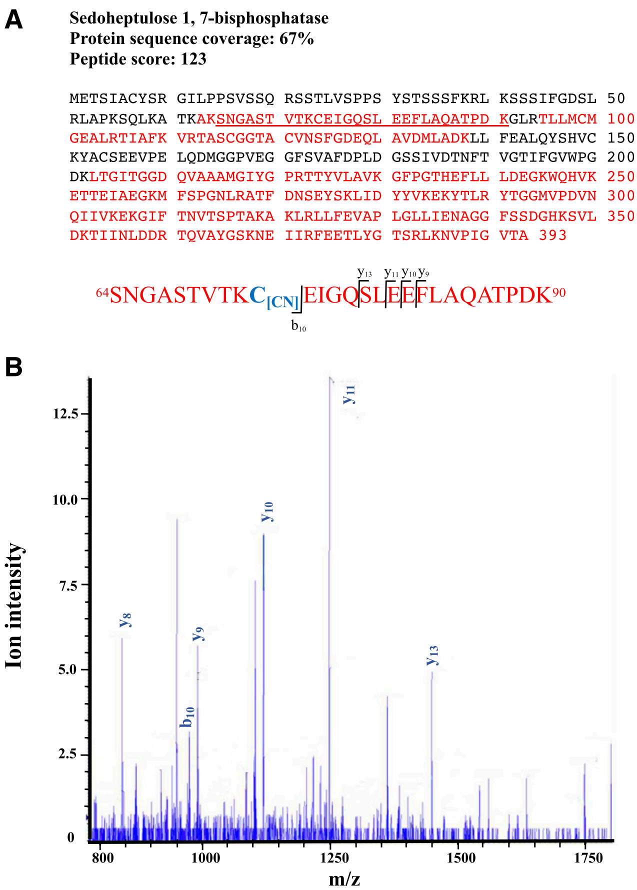

Figure 4. Identification of sedoheptulose 1, 7-bisphosphatase using mass spectrometry. A, The protein was identified with a sequence coverage of 67%. The identified peptides are shown in red, and the peptide containing *S*-cyanylated Cys[74] is underlined. The modified Cys residue is shown in blue color. B, Mass spectrum from the LC-MS/MS analysis of the tryptic peptide containing Cys[74] of SBPase. Predicted ion types and the detected ions are shown in Supplemental Table S11.

hair formation by altering cell wall formation and relaxation at the elongation zone of the hair to prevent its expansion and explains the root hairless phenotype of the *cas-c1* mutant.

The second process identified in which cyanide plays a physiological role is related to the response to pathogens (Chivasa and Carr, 1998; Seo et al., 2011; García et al., 2013). From the GO classification of the proteins that are less abundant or absent in *cas-c1*, we can highlight those involved in signaling, which include 26 proteins of the receptor-like kinase (RLK) family that are conserved signaling components that regulate developmental programs and biotic stresses (Supplemental Fig. S1; Supplemental Table S5; Tang et al., 2017). Among these, there are six Cys-rich RLK DOF26 proteins with a DOF domain, which has four conserved cysteines that may form disulfide bridges as potential targets for thiol redox regulation (Chen, 2001). In addition to the RLKs, many proteins involved in biotic stress are unbalanced in abundance in *cas-c1*, such as the basic-Leu zipper transcription factors POSF21 and WRKY52/RRS1, which confer resistance to *Ralstonia solanacearum* (Williams et al., 2014) and may also explain the increased susceptibility to necrotrophic fungi. The *CAS-C1* mutation also induces the accumulation of a cluster of proteins that include the MAC3B protein, a component of the MOS4-associated complex, which regulates the response to pathogens by regulating *SUPPRESSOR OF NPR1-1 CONSTITUTIVE1* (Monaghan et al., 2009), and the deubiquitinating enzymes UBP12 and UBP13, which regulate the transcription factor MYC2 (Jeong et al., 2017). Therefore, the accumulation of cyanide induces significant transcriptional and proteomic changes in the cell consistent with the alterations in development and pathogen response observed by β-cyano-Ala synthase depletion (García et al., 2013).

Cyanide Posttranslationally Modifies Cys Residues on Proteins

Although cyanide has been proposed to act as a signaling molecule, the mechanism behind this role remains unknown. Based on its chemical reactivity,

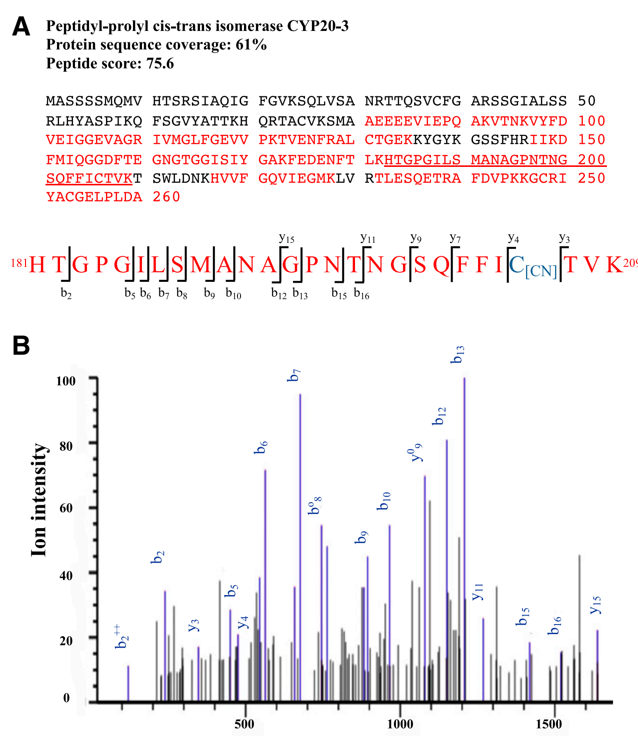

Figure 5. Identification of peptidyl-prolyl cis-trans isomerase CYP20-3 using mass spectrometry. A, The protein was identified with a sequence coverage of 61%. The identified peptides are shown in red, and the peptide containing *S*-cyanylated Cys[206] is underlined. The modified Cys residue is shown in blue color. B, Mass spectrum from the LC-MS/MS analysis of the tryptic peptide containing Cys[206] of CYP20-3. Predicted ion types and the detected ions are shown in Supplemental Table S12.

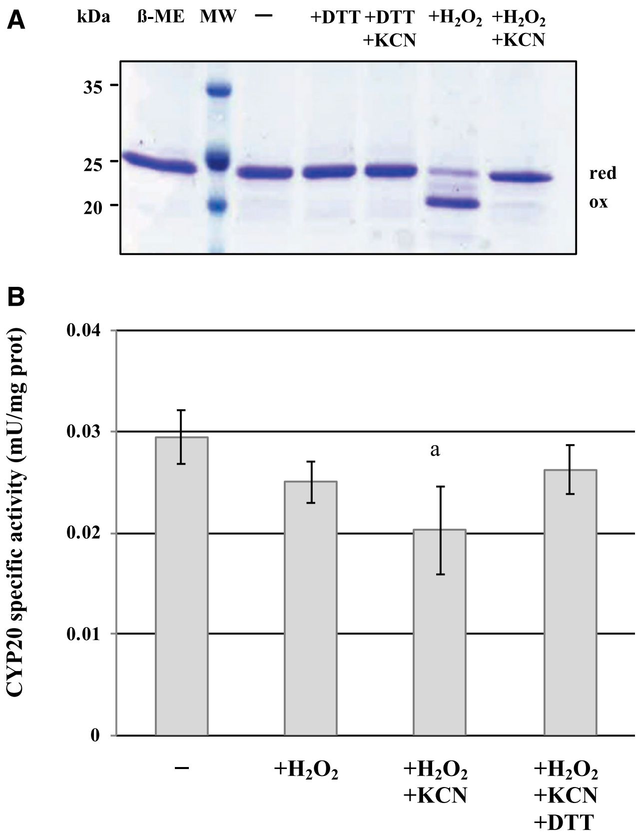

Figure 6. Protein mobility shift and enzymatic activity assays of CYP20-3. A, Alkylation of purified CYP20-3 protein without any treatment (−); after a 20 min treatment with 0.1 mM DTT (+DTT); after a sequential treatment of 20 min with 0.1 mM DTT and 20 additional min with 1 mM KCN (+DTT+KCN); after a treatment of 20 min 0.1 mM H_2O_2 (+H_2O_2); or after a sequential treatment of 20 min 0.1 mM H_2O_2 and additional 20 min with 1 mM KCN (+H_2O_2+KCN). The first lane (+β-ME) corresponds to the nonalkylated, β-mercaptoethanol-reduced protein. MW, molecular weight markers. Reduced (red) and oxidized (ox) forms are indicated. B, Enzymatic activity of purified CYP20-3 protein without any treatment (−); after a 20-min treatment with 0.1 mM H_2O_2 (+H_2O_2); after a sequential treatment of 20 min with 0.1 mM H_2O_2 and 20 additional min with 1 mM KCN (+H_2O_2+KCN); or after a sequential treatment of 20 min with 0.1 mM H_2O_2, 20 additional min with 1 mM KCN (+H_2O_2+KCN), and 20 additional min with 10 mM DTT (+H_2O_2+KCN+DTT). All results are shown as the mean ± SD ($n = 3$). A, Significant differences with control sample ($P < 0.05$, one-way ANOVA).

cyanide can act by forming adducts with the metal centers in proteins that contain iron or cobalt. The cyano-iron complex in the heme prosthetic groups of metalloproteins inhibits the activity of enzymes such as cytochrome c oxidase. A second mechanism involves the posttranslational modification of protein Cys residues leading to the *S*-cyanylation of the protein. This process was thought not to take place under physiological conditions in any organism, however *S*-cyanylated-Cys residues in human plasma proteins, such as immunoglobulin G and serum albumin, are detected after cyanide poisoning or in smoking persons and are used as biomarkers of potential cyanide exposure (Fasco et al., 2007; Grigoryan et al., 2016). We have here identified *S*-cyanylated-Cys residues in the proteins of leaf and root samples, in addition to characterizing the molecular changes produced by genetic β-cyano-Ala synthase depletion and concomitant cyanide accumulation. Using two different physicochemical approaches, the 2-imino-thiazolidine chemical method and direct untargeted analysis of proteins using LC-MS/MS, we found that this modification occurs during physiological growth conditions in leaf and root tissues but can be increased by stimulating the biosynthesis of ethylene and the concomitant cyanide production by treatment with the ACC precursor. Although the number of *S*-cyanylated proteins detected is not high (Table I), we are probably underestimating the true number, since we are only identifying abundant proteins. Many PTMs, such as carbonylation, nitrosylation, persulfuration, or nitration, are identified using chemical labeling methods or by specific antibodies, but so far we do not have available a method to enrich selectively for

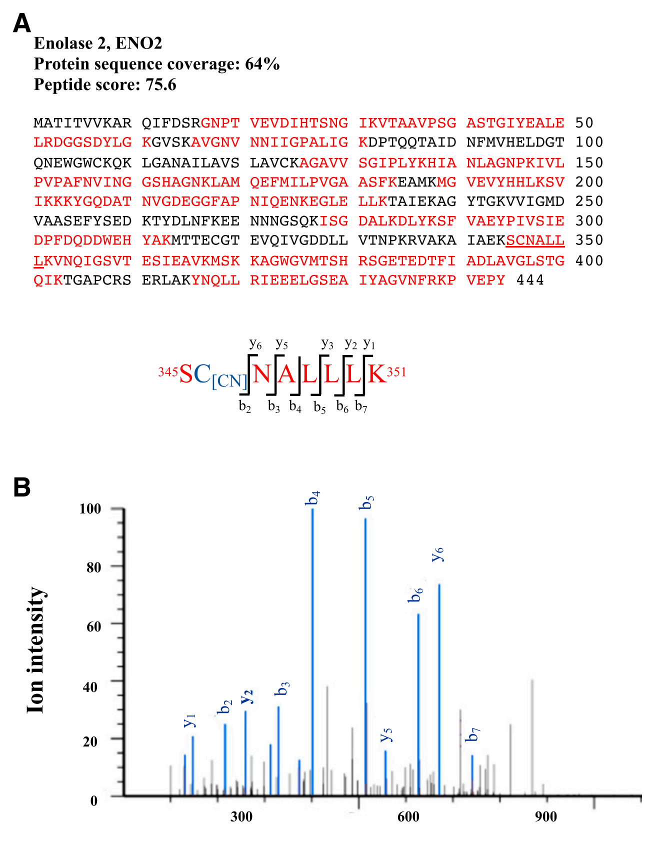

Figure 7. Identification of enolase ENO2 using mass spectrometry. A, The protein was identified with a sequence coverage of 64%. The peptides identified are shown in red, and the peptide containing *S*-cyanylated Cys[346] is underlined. The modified Cys residue is shown in blue color. B, Mass spectrum from LC-MS/MS analysis of the tryptic peptide containing the Cys[346] of ENO2. Predicted ion types and the detected ions are shown in Supplemental Table S13.

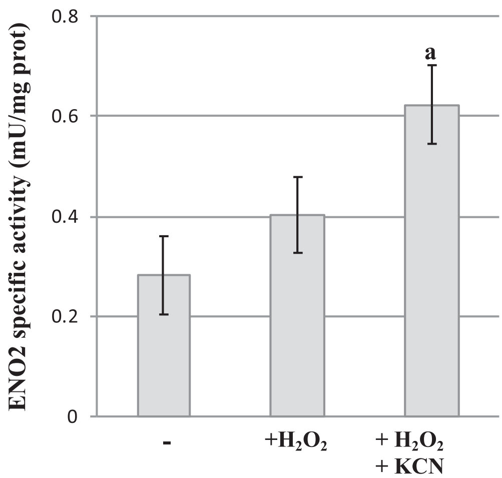

Figure 8. Enzymatic assay of ENO2. Enolase activity of purified ENO2 protein without any treatment (−), after a 20 min treatment with 0.1 mM H_2O_2 (+H_2O_2), or after a sequential treatment of 20 min with 0.1 mM H_2O_2 and 20 additional min with 1 mM KCN (+H_2O_2+KCN). All results are shown as the mean ± SD (n = 6). a, Significant differences with control sample ($P < 0.05$, one-way ANOVA).

S-cyanylated-Cys proteins that will allow us to purify and identify them (Alvarez et al., 2011; Møller et al., 2011; Zhang et al., 2014; Aroca et al., 2017a).

Role of *S*-cyanylation in Cellular Processes

Both methods used to identify the *S*-cyanylated Cys residues detected the ENO2 protein encoded by the *LOS2/ENO2* locus, which functions in glycolysis for the dehydration of 2-phosphoglycerate to produce phosphoenolpyruvate or acts as a repressor of *cMyc* transcription by alternative translation of the locus to produce C-MYC BINDING PROTEIN1 (MBP1; Lee et al., 2002; Eremina et al., 2015). GO classification, enrichment, and clustering analysis of the 163 proteins that were identified to be susceptible to *S*-cyanylation highlighted the role of these proteins in primary carbon fixation, glycolysis, the TCA cycle, and in general, carbon metabolism, but also in chaperone-assisted protein folding and SAM-cycle/DNA methylation (Fig. 9). The in vitro analyses performed with some of the identified *S*-cyanylated proteins showed that *S*-cyanylation of CYP20-3 results in the partial inhibition of its activity but results in the activation of ENO2. Since cyanide action against Cys residue only takes place over oxidized cysteines in the form of disulfide bridges, the effect of *S*-cyanylation depends on the redox state of the target protein. CYP20-3 can form two disulfide bridges, which are required for its isomerase activity and are subject to regulation by thioredoxin (Motohashi et al., 2003), but *S*-cyanylation of Cys-206 in its oxidized state results in the irreversible inactivation of its activity. Most of the enzymes of central carbon metabolism, photosynthetic carbon fixation, glycolysis and the TCA cycle are known to be light/dark regulated; therefore, they are inhibited in the dark by the oxidation of active site cysteines, but reactivated in the light by the action of ferredoxin/thioredoxin systems (Buchanan and Balmer, 2005; Geigenberger et al., 2005). Therefore, cyanide modification of these enzymes in their oxidized state must result in the irreversible inactivation of their activity as shown with CYP20-3. In this case, we can hypothesize that *S*-cyanylation acts as a switch to definitively stop the light/dark regulation of this activity under some specific conditions.

ENO2 activity, the ninth step of glycolysis, is higher during oxidative conditions and during KCN treatment, which indicates that *S*-cyanylation switches on the enzyme activity (Fig. 8; Anderson et al., 1998). Thus, *S*-cyanylation can accelerate the degradation of sugar for ATP production to compensate for the inhibition of the cytochrome oxidase pathway. The *cas-c1* mutant shows higher transcript levels of the alternative oxidase *AOX1a* and higher respiration rates, but the levels of ATP are unaltered (García et al., 2010; Arenas-Alfonseca et al., 2018). Thus, transient cyanide accumulation associated with developmental or environmental stress can potentially generate metabolic perturbations through the inhibition of enzymes of central carbon metabolism and the induction of the AOX gene that controls the production of signaling molecules such as ROS.

A second cyanide signaling mechanism might be the direct effect of *S*-cyanylation on protein localization. Many of the enzymes identified as susceptible to *S*-cyanylation, such as the glycolytic enzymes, including ENO2 and GAPDH, and proteins of the *S*-adenosyl-L-Met (SAM)-cycle, are moonlighting proteins involved either in metabolic pathways and gene transcription, but they lack nuclear localization sequences (Lee et al., 2002; Zaffagnini et al., 2013; Boukouris et al., 2016). Several of the enzymes of the glycolytic pathway are redox regulated and are more active in their reduced form, such as glyceraldehyde 3-phosphate dehydrogenase (Holtgrefe et al., 2008). However, posttranslational modification of the cytosolic GAPDH GapC isoform by *S*-persulfidation of Cys-160 slightly regulates its activity but is critical to determine the cytosolic/nuclear partitioning of the enzyme (Aroca et al., 2015, 2017b). In addition to its enolase activity, the *LOS2/ENO2* locus can be alternatively translated from a second AUG translation initiation codon at position +93 to form the protein MBP1, which was found to bind *c-myc*-like elements in the promoter of the *STZ/ZAT10* gene acting as a transcriptional repressor (Lee et al., 2002). Both ENO2 and MBP1 contain the Cys-346 identified as being susceptible to *S*-cyanylation (Fig. 7). Although we have not tested the effect of *S*-cyanylation in the nuclear localization of ENO2 or the MBP1 protein, previous transcriptomic analyses show the repression of *STZ/ZAT10* in the root tissue of *cas-c1*, suggesting the predominant nuclear localization of MBP1 (García et al., 2010).

In addition to the glycolytic enzymes, we also detected a large number of *S*-cyanylated proteins involved in the

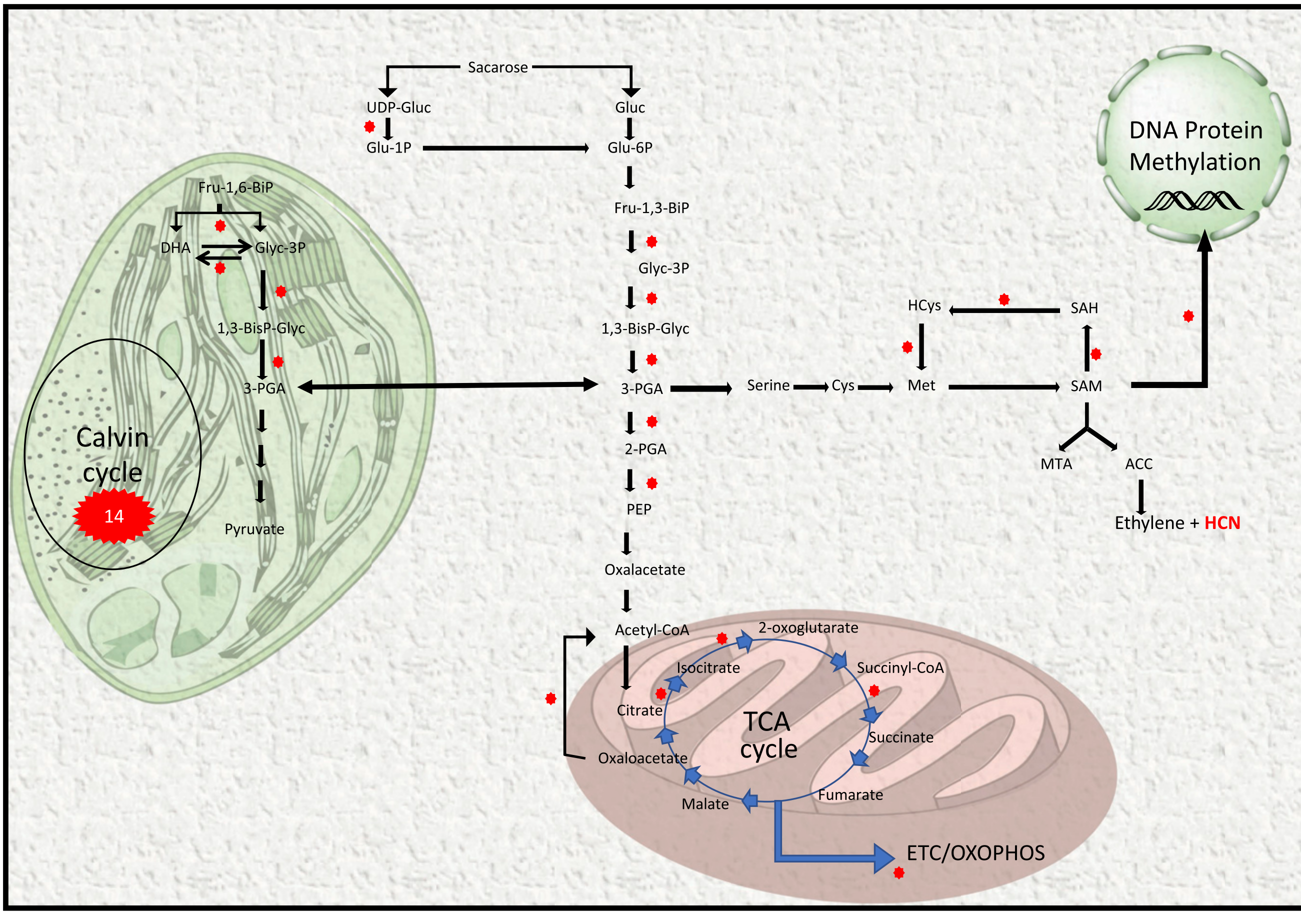

Figure 9. Schematic representation of significant metabolic pathways regulated by *S*-cyanylation. Red stars mark proteins that can be posttranslationally modified by hydrogen cyanide. The number inside the red star at the Calvin cycle represents the number of proteins. TCA, tricarboxylic acid cycle; ETC/OXOPHOS, electron transport chain and oxidative phosphorylation; SAM, *S*-adenosyl Met; SAH, *S*-adenosyl homo-Cys.

SAM cycle and DNA and histone methylation such as Met synthase MS1 and MS2, *S*-adenosyl-L-homo-Cys hydrolase SAHH1/HOG1, SAHH2, and DMT2. Methylation occurs in the nucleus through the metabolite S-adenosyl-Met, which functions as the primary methyl group donor, and the action of methytransferases that transfer the methyl group of SAM producing S-adenosyl-L-homo-Cys (SAH), which is a potent inhibitor of methyltransferase activity (Sauter et al., 2013). SAHH1/HOG is localized either in the cytoplasm or nucleus, but it lacks any nuclear localization signal (Lee et al., 2012). Null transferDNA insertional mutants in *SAHH1*gene, *hog1* mutant, shows embryo-lethal phenotypes (Rocha et al., 2005). However, a *sahh1* mutant that produces the normal SAHH1 protein but in reduced amounts maintains its fertility level but shows a deficiency in root hair development (Wu et al., 2009). Since the *S*-cyanylation of SAHH1 does not result in the severe embryo-lethality of *cas-c1*, the Cys modification may be affecting the nuclear localization of the protein rather than inhibiting the SAHH1 activity. Based on all previous data, we suggest that the effect of *S*-cyanylation on protein localization is plausible and deserves further investigation.

CONCLUSION

In this study, we demonstrate that the accumulation of cyanide by the repression of the β-cyano-Ala synthase activity may induce a nonenzymatic PTM into the Cys motif. Although many nonenzymatic PTMs have been proposed to be indicators of different cellular stresses and used as biomarkers of aging, such as the oxidation of several amino acids, carbonylation or carbamylation, these modifications can also occur in nonstressed and healthy cells and can regulate and influence nonpathogenic cellular processes (Møller et al., 2011; Harmel and Fiedler, 2018). Unlike other nonenzymatic PTMs such as nitrosylation, disulfide formation, and acylation, *S*-cyanylation seems to be a nonreversible modification, since reductants cannot reverse its effect in the analyzed proteins. The fact that *S*-cyanylation occurs on oxidized cysteines in the form of disulfide bridges can cause a change in the properties and function of the proteins. However, a much more extensive study on the effect of this PTM will be necessary to fully understand the functionality of this modification.

MATERIALS AND METHODS

Plant Material and Growth Conditions

Arabidopsis (*Arabidopsis thaliana*) wild type ecotype Col-0 and the *cas-c1* T-DNA insertion mutant (*cas-c1*; SALK_103855; García et al., 2010) were grown in soil in a photoperiod of 16 h of white light (120 μmol m^{-2} s^{-1}) at 20°C and 8 h of dark at 18°C or in hydroponic culture in a photoperiod of 8 h of white light (120 μmol m^{-2} s^{-1}) at 20°C and 16 h of dark at 18°C (Bermúdez et al., 2010). For the hydroponic cultures, seeds were surface-sterilized, incubated for 4 d at 4°C and germinated for 1week in rockwool. Seedlings were introduced in the wells of hydroponic boxes containing 5 L of nutrient solution. The composition of the nutrient solution was as follows: 1 mM KH_2PO_4, 1 mM $MgSO_4 \cdot 7 H_2O$, 15 μM $MnSO_4 \cdot H_2O$, 1 μM $CuSO_4 \cdot 5 H_2O$, 1 μM $ZnSO_4 \cdot 7 H_2O$, 30 μM H_3BO_3, 28 nM $(NH_4)_6Mo_7O_{24} \cdot 4 H_2O$, 100 nM $CoSO_4 \cdot 7 H_2O$, 10 mM $Ca(NO_3)_2 \cdot 4 H_2O$ and 90 mM sequestrene 138 Fe G100 (Syngenta, Spain). All nutrient solutions were changed twice per month.

Mitochondrial Protein Extraction

Mitochondria-enriched samples were isolated from Arabidopsis roots using differential and density-gradient centrifugation as described (Struglics et al., 1993) but with modifications. A total of 30 g of Arabidopsis hydroponic root tissue was ground using a mortar and pestle with liquid nitrogen and resuspended into an extraction buffer containing 15 mM 3-(*N*-morpholino)propanesulfonic acid (MOPS) (pH 7.4), 1.5 mM EDTA, 0.25 M Suc, 0.4% (w/v) bovine serum albumin, and 0.6% (w/v) polyvinylpyrrolidone (PVP-40), using 3 mL of buffer g^{-1} fresh weight, and the homogenates were filtered through two layers of Miracloth (Calbiochem). The filtered homogenate was centrifuged at 2,200*g* for 5 min and the supernatant transferred to a new tube, centrifuged again sequentially at 3,200*g* and 4,500*g* each time for 5 min until a nongreen supernatant was obtained. This final supernatant was centrifuged at 18,000*g* for 30 min. The pellet was resuspended in 1 mL of gradient buffer (20 mM MOPS, pH 7.2, 0.6 M Suc). The separation of the cellular organelles was obtained using a self-generated 45% and 27% Percoll gradient. The gradient was centrifuged at 20,000*g* for 20 min in an ultracentrifuge using an SW28.1 Ti rotor (Beckman) at 4°C. The mitochondrial band was taken out, diluted 10 times with the wash buffer (0.3 M Suc, 1 mM EDTA, 10 mM MOPS at pH 7.2), and centrifuged at 20,000*g* for 15 min four times to wash the organelles free from Percoll. The last pellet was resuspended in 300 μL of lysis buffer (50 mM potassium phosphate buffer, pH 7.0, and 0.1% [v/v] Triton X-100) and the mitochondrial samples disrupted using repeating freeze-thaw cycles and ultrasonic lysis for 1.5 min. The samples were centrifuged at 20,000*g* for 15 min. Proteins from the supernatant were precipitated with 10% (v/v) trichloroacetic acid and ice-cold acetone and resuspended in 20 mM Tris-HCl, pH 8.0.

Identification of Protein *S*-cyanylation Using the 2-Imino-Thiazolidine Chemical Method

Arabidopsis cytosol-enriched leaf protein extract was isolated to perform 2D electrophoresis. For this, 200 mg of frozen leaf tissue was ground in liquid nitrogen using a mortar and pestle. The resulting powder was homogenized in 2 mL of water and ultracentrifuged at 176,000*g* for 1 h at 4°C. The protein concentration in the supernatant was then quantified and used for the ammonium hydroxide treatment. Four hundred micrograms of protein were incubated with 1 M of ammonium hydroxide or 0.01 M of sodium hydroxide for 1 h at 20°C. Proteins were then dried in a speed vacuum, resuspended in 300 μL of 1 mM Tris, 10 mM EDTA, pH 7.5, and precipitated with 10% (v/v) trichloroacetic acid (TCA) overnight at 4°C, centrifuged at 20,000*g* for 15 min at 4°C, and the pellet washed twice with 100% (v/v) acetone. After the final centrifugation step, the protein pellet was air-dried and resolubilized in 8 M urea, 2% (w/v) 3-[(3-cholamidopropyl)dimethylammonio]-1-propanesulfonate hydrate (CHAPS), 50 mM DTT, 0.2% (v/v) ampholytes (Bio-Lyte 3-10 buffer, Bio-Rad), and a trace of bromophenol blue.

The proteins were applied to a linear immobilized pH gradient strip, pH 4 to 7 during rehydration. IEF was performed at 22°C in the Protean IEF Cell (Bio-Rad) in three steps: (1) 250 V for 15 min, (2) 10,000 V for 1 h, and (3) 10,000 V up to 40,000 V. The intensity was fixed at 50 μA per immobilized pH gradient strip to avoid overheating the system. For the second-dimension analysis, the equilibrated gel strips were placed on top of vertical polyacrylamide gels (12% w/v acrylamide and SDS; Laemmli, 1970). Electrophoresis was conducted at 240 V and 35 mA per gel for 5 h using the Protean II xi Cell (Bio-Rad). Protein spots were visualized after Coomassie Brilliant Blue staining.

The 2D images were analyzed using laser densitometry scanning with a GS-800 calibrated densitometer (Bio-Rad), and three high-quality gels from independent protein extracts and conditions were analyzed using the PDQuest software version 7.0 (Bio-Rad). Protein spots of interest were excised, trypsin digested and identified using matrix-assisted laser-desorption ionization-mass spectrometry analysis at the Proteomic Facility of the Institute of Plant Biochemistry and Photosynthesis as previously described (Bermúdez et al., 2012)

Identification of *S*-cyanylated Proteins Using LC-MS/MS Analysis

To identify *S*-cyanylated proteins, tryptic digestion was performed in solution of root extracts, and peptide analysis was carried out using a nano liquid chromatography system coupled to a high-speed mass spectrometer at the Proteomics Facility of the Centro Nacional de Biotecnología, Spain. An aliquot of 40 μg of protein from each treatment group was digested with sequencing-grade modified trypsin (Sigma-Aldrich) at 37°C overnight on a shaker. Three biological replicates for both conditions (wild type and *cas-c1*) were analyzed using the same setup and the parameters previously described (Aroca et al., 2017a).

The mass spectrometry data have been deposited in the ProteomeXchange Consortium via the PRIDE (Vizcaíno et al., 2016) partner repository with the dataset identifier PXD009812.

Protein function analysis and classification was performed using MapMan (Thimm et al., 2004; Klie and Nikoloski, 2012) and clustering analysis by using the STRING database (Szklarczyk et al., 2015). The protein-protein association network was assessed in STRING using interaction evidences coming from experimental data on protein-protein interactions, interaction prediction from coexpression analysis, and known pathways and protein complexes from curated databases and co-occurrence in publications (Szklarczyk et al., 2015, 2017).

Protein Relative Quantitation by SWATH-MS Acquisition and Analysis

Protein samples from mitochondrial extracts for SWATH-MS measurements were alkylated and trypsin-digested as described (Vowinckel et al., 2013; Ortea et al., 2018) and performed at the Proteomic Facility of the Insituto Maimónides de Investigación Biomédica de Córdoba, Spain.

A data dependent acquisition (DDA) approach using nano-LC-MS/MS was first performed to generate the SWATH-MS spectral library as described (Ortea et al., 2018).

The peptide and protein identifications were performed using Protein Pilot software (version 5.0.1, Sciex) with the Paragon algorithm. The searching was conducted against a revised UniProt Swiss-Prot Arabidopsis thaliana protein database (August 2016), specifying iodoacetamide with other possible Cys modifications. The false discovery rate (FDR) was set to 0.01 for both peptides and proteins. The MS/MS spectra of the identified peptides were then used to generate the spectral library for SWATH peak extraction using the add-in for PeakView Software (version 2.1, Sciex) MS/MSALL with SWATH Acquisition MicroApp (version 2.0, Sciex). Peptides with a confidence score above 99% (as obtained from the Protein Pilot database search) were included in the spectral library.

For relative quantitation using SWATH analysis, the same samples used to generate the spectral library were analyzed using a data-independent acquisition method. Each sample (2 μL) was analyzed using the LC-MS equipment and LC gradient described above to build the spectral library but instead used the SWATH-MS acquisition method. The method consisted of repeating a cycle that consisted of the acquisition of 34 TOF MS/MS scans (230 to 1,500 *m/z*, 100 ms acquisition time) of overlapping sequential precursor isolation windows of

25 m/z width (1 m/z overlap) covering the 400 to 1,250 m/z mass range with a previous TOF MS scan (400 to 1250 m/z, 50 ms acquisition time) for each cycle. The total cycle time was 3.5 s.

The targeted data extraction of the fragment ion chromatogram traces from the SWATH runs was performed by PeakView (version 2.1) with the MS/MSALL with SWATH Acquisition MicroApp (version 2.0). This application processed the data using the spectral library created from the shotgun data. Up to 10 peptides per protein and seven fragments per peptide were selected, based on signal intensity. Any shared and modified peptides were excluded from the processing. Windows of 12 min and 0.05 Da width were used to extract the ion chromatograms. SWATH quantitation was attempted for all proteins in the ion library that were identified by ProteinPilot with an FDR below 1%. The extracted ion chromatograms were then generated for each selected fragment ion. The peak areas for the peptides were obtained by summing the peak areas from the corresponding fragment ions. PeakView computed an FDR and a score for each assigned peptide according to the chromatographic and spectral components. Only peptides with an FDR below 5% were used for protein quantitation. Protein quantitation was calculated by adding the peak areas of the corresponding peptides. To test for differential protein abundance between the two groups, MarkerView (version 1.2.1, Sciex) was used for signal normalization.

The mass spectrometry data have been deposited in the ProteomeXchange Consortium via the PRIDE (Vizcaíno et al., 2016) partner repository with the dataset identifier PXD009929.

Expression and Purification of Recombinant His-Tagged Proteins

The complementary DNAs encoding the mature chloroplastic SBPase (At3g55800), the mature chloroplastic CYP20-3 (At3g62030), and the complete cytosolic ENO2 (At2g36530) were cloned into the pDEST17 vector (Invitrogen) with Gateway Technology (Invitrogen) to express an N-terminal 6-His-tagged protein using the *Escherichia coli* expression system. For SBPase and ENO2 protein expression, transformed *E. coli* BL21 cell cultures at an optical density at 600 nm of 0.4 were treated with 0.5 mM isopropyl-β-D-thiogalactopyranoside and incubated for an additional 2 h at 37°C. CYP20-3 was also obtained by isopropyl-β-thiogalactoside induction, but in this case the induction was for 4 h at 30°C. Purification was performed using nickel resin binding under non-denaturing conditions using a Ni-NTA Purification System (Invitrogen) according to the manufacturer's instructions. Recombinant protein production and purification were assessed by SDS-PAGE using 12% (w/v) polyacrylamide gels and Coomassie Brilliant Blue staining.

Electrophoretic Mobility

Nickel-affinity-purified recombinant CYP20-3 was incubated at 4°C with potassium cyanide, hydrogen peroxide, dithiothreitol, or combinations of them for different time periods and different concentrations as indicated, followed by a further incubation with the alkylating agent 2-iodoacetamide at a concentration of 100 mM for 30 min. Subsequently, 20 μg of the samples were subjected to SDS-PAGE using 15% (w/v) polyacrylamide gels, either under nonreducing or reducing conditions depending on the presence of 2-mercaptoethanol in the loading buffer. After electrophoresis, the proteins were visualized using Coomassie Brilliant Blue staining.

Enzyme Activity Assays

The peptidyl-prolyl cis-trans isomerase (PPIase) activity of the nickel-affinity purified recombinant CYP20-3 was measured using a chymotrypsin-coupled assay as previously described (Motohashi et al., 2003) with some modifications. An assay mixture containing 44 mM HEPES-NaOH (pH 8.0), 1 μg of the recombinant CYP20-3 and 0.6 mg of chymotrypsin was incubated for 5 min at 1°C. To initiate the reaction, 75 μM of the substrate *N*-succinyl-Ala-Ala-Pro-Phe-p-nitroanilide (Sigma), previously dissolved in trifluoroethanol and LiCl, was added. The A_{367} was immediately monitored using UV spectrophotometry for 1.5 min. The specific activities were calculated by using the extinction coefficient of 13.4 mM^{-1} cm^{-1}.

The enolase activity of the nickel-affinity purified recombinant ENO2 was measured using a coupled assay system of lactate dehydrogenase and pyruvate kinase. Enolase activity was monitored as a decrease in nicotinamide adenine dinucleotide (NADH) A_{340} and estimated by using the molar extinction coefficient of NADH of 6.22 mM^{-1} cm^{-1} (Fukano and Kimura, 2014).

In all cases, one unit of activity is defined as the amount of enzyme that catalyzed the production of 1 μmol product min^{-1}.

Accession Numbers

Sequence data from this article can be found in the website http://www.arabidopsis.org/ for Arabidopsis genes with locus identifiers provided in this study.

Supplemental Data

The following supplemental materials are available.

Supplemental Figure S1. Schematic image of the signaling pathway and components involved in biotic stress that are absent or less abundant in mitochondrial *cas-c1* samples.

Supplemental Figure S2. Representative diagram of the Calvin cycle and the glycolysis pathway with the proteins identified as *S*-cyanylated in leaf and root tissues.

Supplemental Table S1. Overrepresentation test in mitochondrial proteins identified in the spectral library in mitochondrial samples.

Supplemental Table S2. Proteins with different abundance in mitochondrial samples between wild type and *cas-c1* with $P < 0.05$.

Supplemental Table S3. Identified proteins in the spectral library only present in mitochondrial wild-type samples and absent in *cas-c1*.

Supplemental Table S4. Identified proteins in the spectral library only present in mitochondrial *cas-c1* samples and absent in wild type.

Supplemental Table S5. Functional classification of less abundant or absent proteins in mitochondrial *cas-c1* samples.

Supplemental Table S6. Functional classification of proteins more abundant or only present in mitochondrial *cas-c1* samples.

Supplemental Table S7. Overrepresentation test of the more abundant proteins in mitochondrial *cas-c1* samples.

Supplemental Table S8. *S*-cyanylated proteins identified in wild-type and *cas-c1* leaves as determined by the chemical 2-imino-thiazolidine method.

Supplemental Table S9. Overrepresentation test of *S*-cyanylated proteins identified in wild-type and *cas-c1* leaves.

Supplemental Table S10. Total proteins identified as susceptible to *S*-cyanylation in leaf and root tissues.

Supplemental Table S11. SBPase predicted ion types for *S*-cyanyl modified peptide.

Supplemental Table S12. CYP20-3 predicted ion types for the modified peptide.

Supplemental Table S13. ENO2 predicted ion types for the modified peptide.

Supplemental Dataset S1. Proteins identified by shotgun data dependent acquisition in mitochondrial samples.

Supplemental Dataset S2. Quantified proteins using the SWATH acquisition method in mitochondrial samples.

Supplemental Dataset S3. Identified proteins in ACC treated (R^+) and untreated (R^-) root samples.

ACKNOWLEDGMENTS

We thank the European Regional Development Fund through the Agencia Estatal de Investigación for financial support. We also thanks Rocio Rodríguez from the Proteomic Facility at IBVF, Angeles Aroca, and Ignacio Ortea from IMIBIC for their technical advice.

Received September 4, 2018; accepted October 23, 2018; published October 30, 2018.

LITERATURE CITED

Alvarez C, Lozano-Juste J, Romero LC, García I, Gotor C, León J (2011) Inhibition of Arabidopsis O-acetylserine(thiol)lyase A1 by tyrosine nitration. J Biol Chem **286:** 578–586

Álvarez C, García I, Romero LC, Gotor C (2012) Mitochondrial sulfide detoxification requires a functional isoform O-acetylserine(thiol)lyase C in *Arabidopsis thaliana*. Mol Plant **5:** 1217–1226

Anderson LE, Li AD, Stevens FJ (1998) The enolases of ice plant and Arabidopsis contain a potential disulphide and are redox sensitive. Phytochemistry **47:** 707–713

Arenas-Alfonseca L, Gotor C, Romero LC, García I (2018) β-cyanoalanine synthase action in root hair elongation is exerted at early steps of the root hair elongation pathway and is independent of direct cyanide inactivation of NADPH oxidase. Plant Cell Physiol **59:** 1072–1083

Aroca A, Benito JM, Gotor C, Romero LC (2017a) Persulfidation proteome reveals the regulation of protein function by hydrogen sulfide in diverse biological processes in Arabidopsis. J Exp Bot **68:** 4915–4927

Aroca A, Schneider M, Scheibe R, Gotor C, Romero LC (2017b) Hydrogen sulfide regulates the cytosolic/nuclear partitioning of glyceraldehyde-3-phosphate dehydrogenase by enhancing its nuclear localization. Plant Cell Physiol **58:** 983–992

Aroca A, Gotor C, Romero LC (2018) Hydrogen sulfide signaling in plants: Emerging roles of protein persulfidation. Front Plant Sci **9:** 1369

Aroca Á, Serna A, Gotor C, Romero LC (2015) S-sulfhydration: A cysteine posttranslational modification in plant systems. Plant Physiol **168:** 334–342

Baskar V, Park SW, Nile SH (2016) An update on potential perspectives of glucosinolates on protection against microbial pathogens and endocrine dysfunctions in humans. Crit Rev Food Sci Nutr **56:** 2231–2249

Berg SP, Krogmann DW (1975) Mechanism of KCN inhibition of photosystem I. J Biol Chem **250:** 8957–8962

Bermúdez MA, Páez-Ochoa MA, Gotor C, Romero LC (2010) Arabidopsis S-sulfocysteine synthase activity is essential for chloroplast function and long-day light-dependent redox control. Plant Cell **22:** 403–416

Bermúdez MA, Galmés J, Moreno I, Mullineaux PM, Gotor C, Romero LC (2012) Photosynthetic adaptation to length of day is dependent on S-sulfocysteine synthase activity in the thylakoid lumen. Plant Physiol **160:** 274–288

Bethke PC, Libourel IG, Reinöhl V, Jones RL (2006) Sodium nitroprusside, cyanide, nitrite, and nitrate break Arabidopsis seed dormancy in a nitric oxide-dependent manner. Planta **223:** 805–812

Bishop NI, Spikes JD (1955) Inhibition by cyanide of the photochemical activity of isolated chloroplasts. Nature **176:** 307–308

Böttcher C, Westphal L, Schmotz C, Prade E, Scheel D, Glawischnig E (2009) The multifunctional enzyme CYP71B15 (PHYTOALEXIN DEFICIENT3) converts cysteine-indole-3-acetonitrile to camalexin in the indole-3-acetonitrile metabolic network of Arabidopsis thaliana. Plant Cell **21:** 1830–1845

Boukouris AE, Zervopoulos SD, Michelakis ED (2016) Metabolic enzymes moonlighting in the nucleus: Metabolic regulation of gene transcription. Trends Biochem Sci **41:** 712–730

Buchanan BB, Balmer Y (2005) Redox regulation: A broadening horizon. Annu Rev Plant Biol **56:** 187–220

Catsimpoolas N, Wood JL (1966) Specific cleavage of cystine peptides by cyanide. J Biol Chem **241:** 1790–1796

Chen Z (2001) A superfamily of proteins with novel cysteine-rich repeats. Plant Physiol **126:** 473–476

Chivasa S, Carr JP (1998) Cyanide restores N gene-mediated resistance to tobacco mosaic virus in transgenic tobacco expressing salicylic acid hydroxylase. Plant Cell **10:** 1489–1498

Cohen WS, McCarty RE (1976) Reversibility of the cyanide inhibition of electron transport in spinach chloroplast thylakoids. Biochem Biophys Res Commun **73:** 679–685

Eremina M, Rozhon W, Yang S, Poppenberger B (2015) ENO2 activity is required for the development and reproductive success of plants, and is feedback-repressed by AtMBP-1. Plant J **81:** 895–906

Fasco MJ, Hauer III CR, Stack RF, O'hehir C, Barr JR, Eadon GA (2007) Cyanide adducts with human plasma proteins: Albumin as a potential exposure surrogate. Chem Res Toxicol **20:** 677–684

Fricker LD (2015) Limitations of mass spectrometry-based peptidomic approaches. J Am Soc Mass Spectrom **26:** 1981–1991

Fukano K, Kimura K (2014) Measurement of enolase activity in cell lysates. Methods Enzymol **542:** 115–124

García I, Castellano JM, Vioque B, Solano R, Gotor C, Romero LC (2010) Mitochondrial beta-cyanoalanine synthase is essential for root hair formation in Arabidopsis thaliana. Plant Cell **22:** 3268–3279

García I, Rosas T, Bejarano ER, Gotor C, Romero LC (2013) Transient transcriptional regulation of the CYS-C1 gene and cyanide accumulation upon pathogen infection in the plant immune response. Plant Physiol **162:** 2015–2027

García I, Gotor C, Romero LC (2014) Beyond toxicity: A regulatory role for mitochondrial cyanide. Plant Signal Behav **9:** e27612

Gawron O (1966) Chapter 14 - On the reaction of cyanide with cystine and cystine peptides. *In* N Kharasch, CY Meyers, eds, The Chemistry of Organic Sulfur Compounds. Oxford, Pergamon, pp 351–365

Geigenberger P, Kolbe A, Tiessen A (2005) Redox regulation of carbon storage and partitioning in response to light and sugars. J Exp Bot **56:** 1469–1479

Giegé P, Heazlewood JL, Roessner-Tunali U, Millar AH, Fernie AR, Leaver CJ, Sweetlove LJ (2003) Enzymes of glycolysis are functionally associated with the mitochondrion in Arabidopsis cells. Plant Cell **15:** 2140–2151

Gotor C, Laureano-Marín AM, Arenas-Alfonseca L, Moreno I, Aroca Á, García I, Romero LC (2017). Advances in plant sulfur metabolism and signaling. *In* FM Canovas, U Lüttge, R Matyssek, eds, Progress in Botany, **Vol 78**, Cham, Switzerland, Springer International Publishing, pp 45–66

Grierson C, Nielsen E, Ketelaarc T, Schiefelbein J (2014) Root hairs. Arabidopsis Book **12:** e0172

Grigoryan H, Edmands W, Lu SS, Yano Y, Regazzoni L, Iavarone AT, Williams ER, Rappaport SM (2016) Adductomics pipeline for untargeted analysis of modifications to Cys34 of human serum albumin. Anal Chem **88:** 10504–10512

Hanschen FS, Lamy E, Schreiner M, Rohn S (2014) Reactivity and stability of glucosinolates and their breakdown products in foods. Angew Chem Int Ed Engl **53:** 11430–11450

Harmel R, Fiedler D (2018) Features and regulation of non-enzymatic post-translational modifications. Nat Chem Biol **14:** 244–252

Hatzfeld Y, Maruyama A, Schmidt A, Noji M, Ishizawa K, Saito K (2000) beta-Cyanoalanine synthase is a mitochondrial cysteine synthase-like protein in spinach and Arabidopsis. Plant Physiol **123:** 1163–1171

Holtgrefe S, Gohlke J, Starmann J, Druce S, Klocke S, Altmann B, Wojtera J, Lindermayr C, Scheibe R (2008) Regulation of plant cytosolic glyceraldehyde 3-phosphate dehydrogenase isoforms by thiol modifications. Physiol Plant **133:** 211–228

Isom GE, Way JL (1984) Effects of oxygen on the antagonism of cyanide intoxication: cytochrome oxidase, in vitro. Toxicol Appl Pharmacol **74:** 57–62

Jeong JS, Jung C, Seo JS, Kim JK, Chua NH (2017) The deubiquitinating enzymes UBP12 and UBP13 positively regulate MYC2 levels in jasmonate responses. Plant Cell **29:** 1406–1424

Klie S, Nikoloski Z (2012) The choice between MapMan and gene ontology for automated gene function prediction in plant science. Front Genet **3:** 115

Knowles CJ (1976) Microorganisms and cyanide. Bacteriol Rev **40:** 652–680

Laemmli UK (1970) Cleavage of structural proteins during the assembly of the head of bacteriophage T4. Nature **227:** 680–685

Lee H, Guo Y, Ohta M, Xiong L, Stevenson B, Zhu JK (2002) LOS2, a genetic locus required for cold-responsive gene transcription encodes a bi-functional enolase. EMBO J **21:** 2692–2702

Lee S, Doxey AC, McConkey BJ, Moffatt BA (2012) Nuclear targeting of methyl-recycling enzymes in Arabidopsis thaliana is mediated by specific protein interactions. Mol Plant **5:** 231–248

Lozano-Durán R, García I, Huguet S, Aubourg-Balzergue S, Romero LC, Bejarano ER (2012) Geminivirus C2 protein represses genes involved in sulphur assimilation and this effect can be counteracted by jasmonate treatment. Eur J Plant Pathol **134:** 49–59

Mi H, Huang X, Muruganujan A, Tang H, Mills C, Kang D, Thomas PD (2017) PANTHER version 11: Expanded annotation data from Gene Ontology and Reactome pathways, and data analysis tool enhancements. Nucleic Acids Res **45**(D1): D183–D189

Møller IM, Rogowska-Wrzesinska A, Rao RS (2011) Protein carbonylation and metal-catalyzed protein oxidation in a cellular perspective. J Proteomics **74:** 2228–2242

Monaghan J, Xu F, Gao M, Zhao Q, Palma K, Long C, Chen S, Zhang Y, Li X (2009) Two Prp19-like U-box proteins in the MOS4-associated complex play redundant roles in plant innate immunity. PLoS Pathog **5:** e1000526

Motohashi K, Koyama F, Nakanishi Y, Ueoka-Nakanishi H, Hisabori T (2003) Chloroplast cyclophilin is a target protein of thioredoxin. Thiol modulation of the peptidyl-prolyl cis-trans isomerase activity. J Biol Chem **278:** 31848–31852

Nguema-Ona E, Bannigan A, Chevalier L, Baskin TI, Driouich A (2007) Disruption of arabinogalactan proteins disorganizes cortical microtubules in the root of Arabidopsis thaliana. Plant J **52:** 240–251

Nicholls P, Marshall DC, Cooper CE, Wilson MT (2013) Sulfide inhibition of and metabolism by cytochrome c oxidase. Biochem Soc Trans **41:** 1312–1316

Ortea I, Ruiz-Sánchez I, Cañete R, Caballero-Villarraso J, Cañete MD (2018) Identification of candidate serum biomarkers of childhood-onset growth hormone deficiency using SWATH-MS and feature selection. J Proteomics **175:** 105–113

Park C-M, Weerasinghe L, Day JJ, Fukuto JM, Xian M (2015) Persulfides: Current knowledge and challenges in chemistry and chemical biology. Mol Biosyst **11:** 1775–1785

Peiser GD, Wang TT, Hoffman NE, Yang SF, Liu HW, Walsh CT (1984) Formation of cyanide from carbon 1 of 1-aminocyclopropane-1-carboxylic acid during its conversion to ethylene. Proc Natl Acad Sci USA **81:** 3059–3063

Rao RSP, Salvato F, Thal B, Eubel H, Thelen JJ, Møller IM (2017) The proteome of higher plant mitochondria. Mitochondrion **33:** 22–37

Ressler C, Giza YH, Nigam SN (1969) β-cyanoalanine, product of cyanide fixation and intermediate in asparagine biosynthesis in certain species of Lathyrus and Vicia. J Am Chem Soc **91:** 2766–2775

Rocha PS, Sheikh M, Melchiorre R, Fagard M, Boutet S, Loach R, Moffatt B, Wagner C, Vaucheret H, Furner I (2005) The Arabidopsis HOMOLOGY-DEPENDENT GENE SILENCING1 gene codes for an S-adenosyl-L-homocysteine hydrolase required for DNA methylation-dependent gene silencing. Plant Cell **17:** 404–417

Romero LC, Aroca MA, Laureano-Marín AM, Moreno I, García I, Gotor C (2014) Cysteine and cysteine-related signaling pathways in *Arabidopsis thaliana*. Mol Plant **7:** 264–276

Salvato F, Havelund JF, Chen M, Rao RSP, Rogowska-Wrzesinska A, Jensen ON, Gang DR, Thelen JJ, Møller IM (2014) The potato tuber mitochondrial proteome. Plant Physiol **164:** 637–653

Sauter M, Moffatt B, Saechao MC, Hell R, Wirtz M (2013) Methionine salvage and S-adenosylmethionine: essential links between sulfur, ethylene and polyamine biosynthesis. Biochem J **451:** 145–154

Seo S, Mitsuhara I, Feng J, Iwai T, Hasegawa M, Ohashi Y (2011) Cyanide, a coproduct of plant hormone ethylene biosynthesis, contributes to the resistance of rice to blast fungus. Plant Physiol **155:** 502–514

Struglics A, Fredlund KM, Rasmusson AG, Møller IM (1993) The presence of a short redox chain in the membrane of intact potato tuber peroxisomes and the association of malate dehydrogenase with the peroxisomal membrane. Physiol Plant **88:** 19–28

Szklarczyk D, Franceschini A, Wyder S, Forslund K, Heller D, Huerta-Cepas J, Simonovic M, Roth A, Santos A, Tsafou KP, et al (2015) STRING v10: Protein-protein interaction networks, integrated over the tree of life. Nucleic Acids Res **43:** D447–D452

Szklarczyk D, Morris JH, Cook H, Kuhn M, Wyder S, Simonovic M, Santos A, Doncheva NT, Roth A, Bork P, et al (2017) The STRING database in 2017: Quality-controlled protein-protein association networks, made broadly accessible. Nucleic Acids Res **45**(D1): D362–D368

Tang D, Wang G, Zhou J-M (2017) Receptor kinases in plant-pathogen interactions: More than pattern recognition. Plant Cell **29:** 618–637

Taylorson RB, Hendricks SB (1973) Promotion of seed germination by cyanide. Plant Physiol **52:** 23–27

Thimm O, Bläsing O, Gibon Y, Nagel A, Meyer S, Krüger P, Selbig J, Müller LA, Rhee SY, Stitt M (2004) MAPMAN: A user-driven tool to display genomics data sets onto diagrams of metabolic pathways and other biological processes. Plant J **37:** 914–939

Thompson JP, Marrs TC (2012). Hydroxocobalamin in cyanide poisoning. Clin Toxicol (Phila) **50:** 875–885

Tinajero-Trejo M, Jesse HE, Poole RK (2013) Gasotransmitters, poisons, and antimicrobials: It's a gas, gas, gas! F1000Prime Rep **5:** 28

Trebst AV, Losada M, Arnon DI (1960) Photosynthesis by isolated chloroplasts. XII. Inhibitors of carbon dioxide assimilation in a reconstituted chloroplast system. J Biol Chem **235:** 840–844

Vizcaíno JA, Csordas A, del-Toro N, Dianes JA, Griss J, Lavidas I, Mayer G, Perez-Riverol Y, Reisinger F, Ternent T, et al (2016) 2016 update of the PRIDE database and its related tools. Nucleic Acids Res **44**(D1): D447–D456

Vowinckel J, Capuano F, Campbell K, Deery MJ, Lilley KS, Ralser M (2013) The beauty of being (label)-free: sample preparation methods for SWATH-MS and next-generation targeted proteomics. F1000 Res **2:** 272

Wagner ES, Davis RE (1966) Displacement reactions. IX. The reaction of cyanide ion with cystine. An example of amino group participation as detected with nitrogen-15 during cleavage of a sulfur-sulfur Bond1. J Am Chem Soc **88:** 7–12

Wang R (2014) Gasotransmitters: Growing pains and joys. Trends Biochem Sci **39:** 227–232

Williams SJ, Sohn KH, Wan L, Bernoux M, Sarris PF, Segonzac C, Ve T, Ma Y, Saucet SB, Ericsson DJ, et al (2014) Structural basis for assembly and function of a heterodimeric plant immune receptor. Science **344:** 299–303

Wong CE, Carson RA, Carr JP (2002) Chemically induced virus resistance in *Arabidopsis thaliana* is independent of pathogenesis-related protein expression and the NPR1 gene. Mol Plant Microbe Interact **15:** 75–81

Wu X, Li F, Kolenovsky A, Caplan A, Cui Y, Cutler A, Tsang EWT (2009) A mutant deficient in S-adenosylhomocysteine hydrolase in Arabidopsis shows defects in root-hair development. Botany **87:** 571–584

Yamasaki H, Watanabe NS, Sakihama Y, Cohen MF (2016) An overview of methods in plant nitric oxide (NO) research: Why do we always need to use multiple methods? Methods Mol Biol **1424:** 1–14

Yip WK, Yang SF (1988) Cyanide metabolism in relation to ethylene production in plant tissues. Plant Physiol **88:** 473–476

Zaffagnini M, Fermani S, Costa A, Lemaire SD, Trost P (2013) Plant cytoplasmic GAPDH: Redox post-translational modifications and moonlighting properties. Front Plant Sci **4:** 450

Zhang D, Macinkovic I, Devarie-Baez NO, Pan J, Park CM, Carroll KS, Filipovic MR, Xian M (2014) Detection of protein S-sulfhydration by a tag-switch technique. Angew Chem Int Ed Engl **53:** 575–581

Zidenga T, Siritunga D, Sayre RT (2017) Cyanogen metabolism in cassava roots: Impact on protein synthesis and root development. Front Plant Sci **8:** 220